TECHNICAL MEMORANDUM

659

Prognostic Aerosols in the ECMWF IFS: MACC vs. GEMS Aerosols

J.-J. Morcrette, A. Benedetti, L. Jones,
J.W. Kaiser, M. Razinger, M. Suttie

European Centre for Medium-Range Weather Forecasts, Reading, UK

Research Department

December 2011

European Centre for Medium-Range Weather Forecasts
Europäisches Zentrum für mittelfristige Wettervorhersage
Centre européen pour les prévisions météorologiques à moyen terme

Series: ECMWF Technical Memoranda

A full list of ECMWF Publications can be found on our web site under:
http://www.ecmwf.int/publications/

Contact: library@ecmwf.int

European Centre for Medium-Range Weather Forecasts
Shinfield Park, Reading, RG2 9AX, England

Abstract

Prognostic aerosols were experimentally introduced in the ECMWF Integrated Forecasting System as part of the GEMS project in 2005. Their representation was refined as part of the MACC project, starting in 2009. Differences between the two systems are first discussed and results of comparisons of aerosol optical depth with satellite and AERONET ground station observations are discussed.

1 Introduction

Nowadays, most of the GCMs used for climate studies have included a description of aerosols and of their effects on radiation and cloud fields. If prognostic aerosols in climate GCMs are now standard features, their introduction in global weather forecast models is much more recent. The model from the European Centre for Medium-range Weather Forecasts (ECMWF) has had since the 1980s a climatological representation of the main aerosol types, first from Tanré et al. (1984), which was superseded in 2003 by climatologies derived as monthly means from chemical-transport model simulations (Tegen et al., 1997). At the time, such a change in aerosol climatologies was shown to be able to affect the meteorology both locally (Tompkins et al., 2005) and remotely through teleconnections (Rodwell and Jung, 2008).

As part of the GEMS project (Global and regional Earth-system Monitoring using Satellite and in-situ data; Hollingsworth et al., 2008), the ECMWF has developed its assimilation system to include observations pertaining to greenhouse gases, reactive gases and aerosols. In the ECMWF/GEMS configuration, the Integrated Forecast System (IFS) in the computation of the trajectory forecast used in the assimilation, has been extended to include a number of tracers, which are advected by the model dynamics and interact with the various physical processes.

ECMWF first produced a reanalysis for the years 2003 to 2008, then from July 2008 used the same experimental system for pre-operational near-real time analysis and forecast (see GEMS web address in reference). With respect to the aerosols, sources have thus been added to the model, and a representation of the aerosol physical processes (namely the interactions of the aerosols with the vertical diffusion and the convection, plus the sedimentation, dry deposition and wet deposition by large-scale and convective precipitation) are now part of the package of physical parametrisations of the ECMWF IFS model (Morcrette et al., 2009). Details of the analysis of MODIS data to constrain the initial values of the aerosols at the start of the forecasts can be found in Benedetti et al. (2009).

During GEMS, the aerosols were not interactive with either the model radiative or cloud processes, and the radiation fields were computed using the monthly mean climatological distributions of aerosol. As part of the follow-up MACC project (Monitoring Atmospheric Composition and Climate; Simmons, 2010), the aerosol analysis and forecast system has been further developed to allow the prognostic aerosols to interact with the rest of the model. Results for this study are presented in another paper. Here we only compare the aerosols produced by the MACC analysis and subsequent forecasts to similar aerosol parameters produced during GEMS.

Section 2 quickly describes the various model configurations used in the study. Results are presented in Section 3. Conclusions and perspectives are discussed in Section 4.

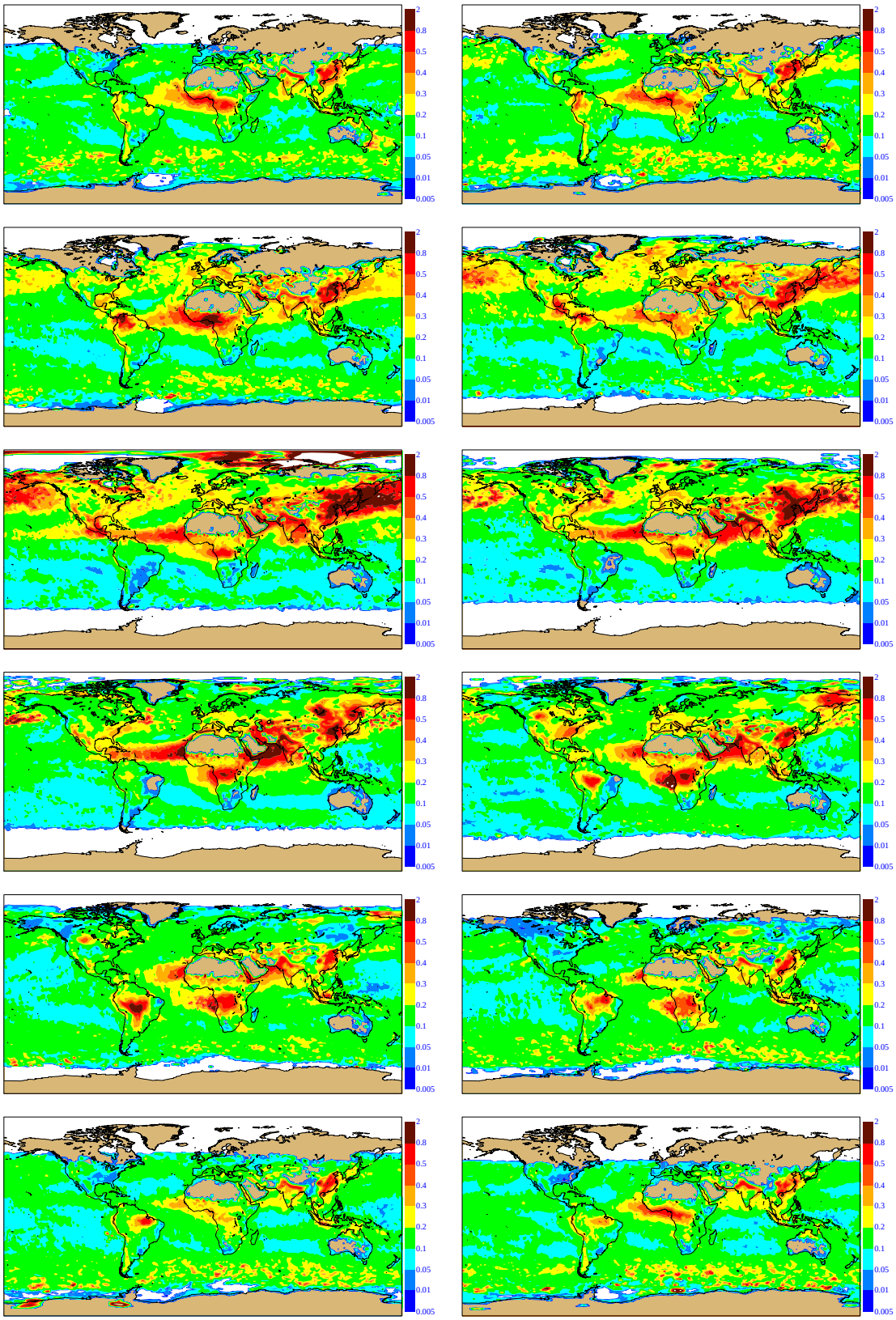

Figure 1: The month-by-month total aerosol optical depth for 2003, derived from the MODIS spectroradiometer on the Aqua satellite. January is top left, February is top right, other months follow in a similar way.

2 Model description and experimental design

A detailed description of the ECMWF forecast model including aerosol processes is given in Morcrette et al. (2009).

The initial package of ECMWF physical parametrisations dedicated to aerosol processes mainly follows the aerosol treatment in the LOA/LMD-Z model (Laboratoire d'Optique Atmosphérique/Laboratoire de Météorologie Dynamique: Boucher et al., 2002, Reddy et al., 2005). Five types of tropospheric aerosols are considered: sea salt, dust, organic and black carbon, and sulphate aerosols. A prognostic representation of the stratospheric aerosols is not included here, as it was not part of GEMS and was not available to be included in MACC. Instead, the stratospheric aerosols are the climatological ones available as part of the ECMWF operational IFS. In the following, all results correspond to a version of the ECMWF model with prognostic tropospheric aerosols and climatological stratospheric aerosols. Similarly, the emission of aerosols by volcanoes is not present in the following results. Both types of aerosols will be considered in a later stage of the introduction of aerosols in the ECMWF IFS.

For all tropospheric aerosols, sources are defined, the sedimentation of all particles, and the wet and dry deposition processes are represented. For organic matter (OM) and black carbon (BC), two components, hydrophobic and hydrophilic, are considered, and the transfer from hydrophobic to hydrophilic is also included. The sulphur cycle is considered via a precursor variable SO_2 transformed in a sulphate aerosol (SO_4) with a time-scale simply dependent on latitude (as in Huneeus and Boucher, 2007).

A bin representation is used in this study to include prognostic aerosols of natural origin (taken to mean sea-salt SS and dust DU). The maximum flexibility regarding the limits of the bins for the sea-salt and dust aerosols is allowed in the model. In the following, the sea-salt aerosols are tentatively represented by 3 bins, with limits at 0.03, 0.5, 5 and 20 microns. Similarly, the desert dust aerosols are represented by 3 bins with limits at 0.03, 0.55, 0.9, and 20 microns. The above limits are chosen so that roughly 10, 20 and 70 percent of the total mass of each aerosol type are in the various bins.

The natural aerosols (SS, DU and dimethyl-sulphide DMS) have their sources only linked to some prognostic and diagnostic model variables. In contrast, the anthropogenic aerosols (organic matter OM, black carbon BC and SO_4) have their sources read from external data-sets. Sources of sea-salt and desert dust are interactive with surface and near-surface variables of the model. Sources for the other aerosol types linked to emissions from domestic, industrial, power generation, transport and shipping activities, are taken either from the GFED (Global Fire Emission Database), SPEW (Speciated Particulate Emission Wizard), and EDGAR (Emission Database for Global Atmospheric Research) annual- or monthly-mean climatologies. More details on the sources of these aerosols are given in Dentener et al. (2006). Emissions of OM, BC and SO_2 linked to fire emissions are obtained using the analysis of MODIS and SEVIRI satellite observations, with GEMS using GFEDv2 and MACC using GFEDv3.0 (Kaiser et al., 2009, 2011).

Several types of removal processes are considered, i/ the dry deposition including the turbulent transfer to the surface, ii/ the gravitational settling, and iii/ the wet deposition including rainout (by large-scale and convective precipitation) and washout of aerosol particles in and below the clouds. The wet and dry deposition schemes are standard, whereas the sedimentation of aerosols follows closely what was introduced by Tompkins (2005) for the sedimentation of ice particles. Hygroscopic effects are also considered for organic matter and black carbon aerosols.

Compared to the climatological aerosols, the prognostic aerosols display an increased temporal, horizontal and vertical variability, and each of the aerosol components may now directly respond to the variations in relative humidity.

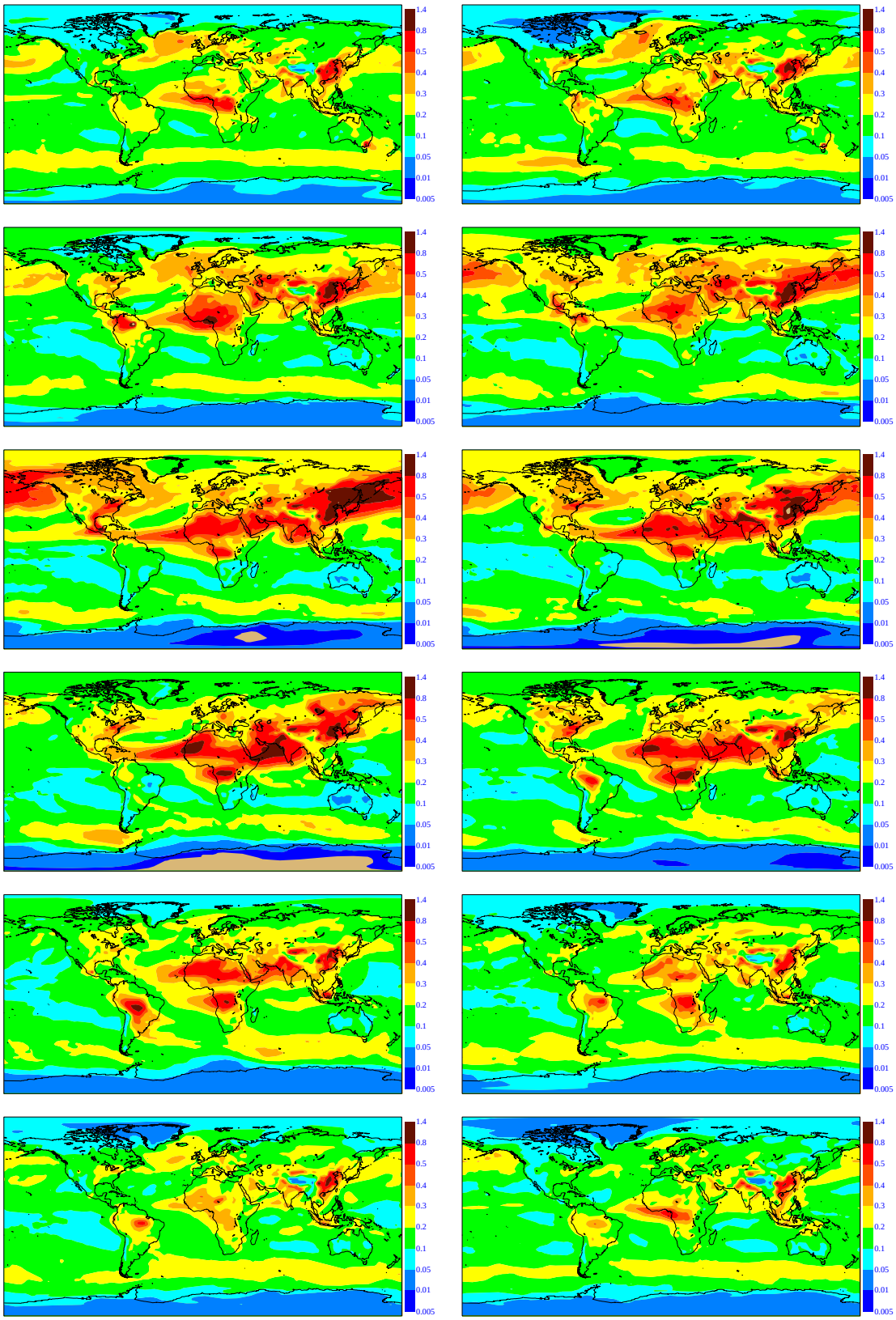

Figure 2: The month-by-month total aerosol optical depth for 2003, from the GEMS aerosol reanalysis (see text). January is top left, February is top right, other months follow in a similar way.

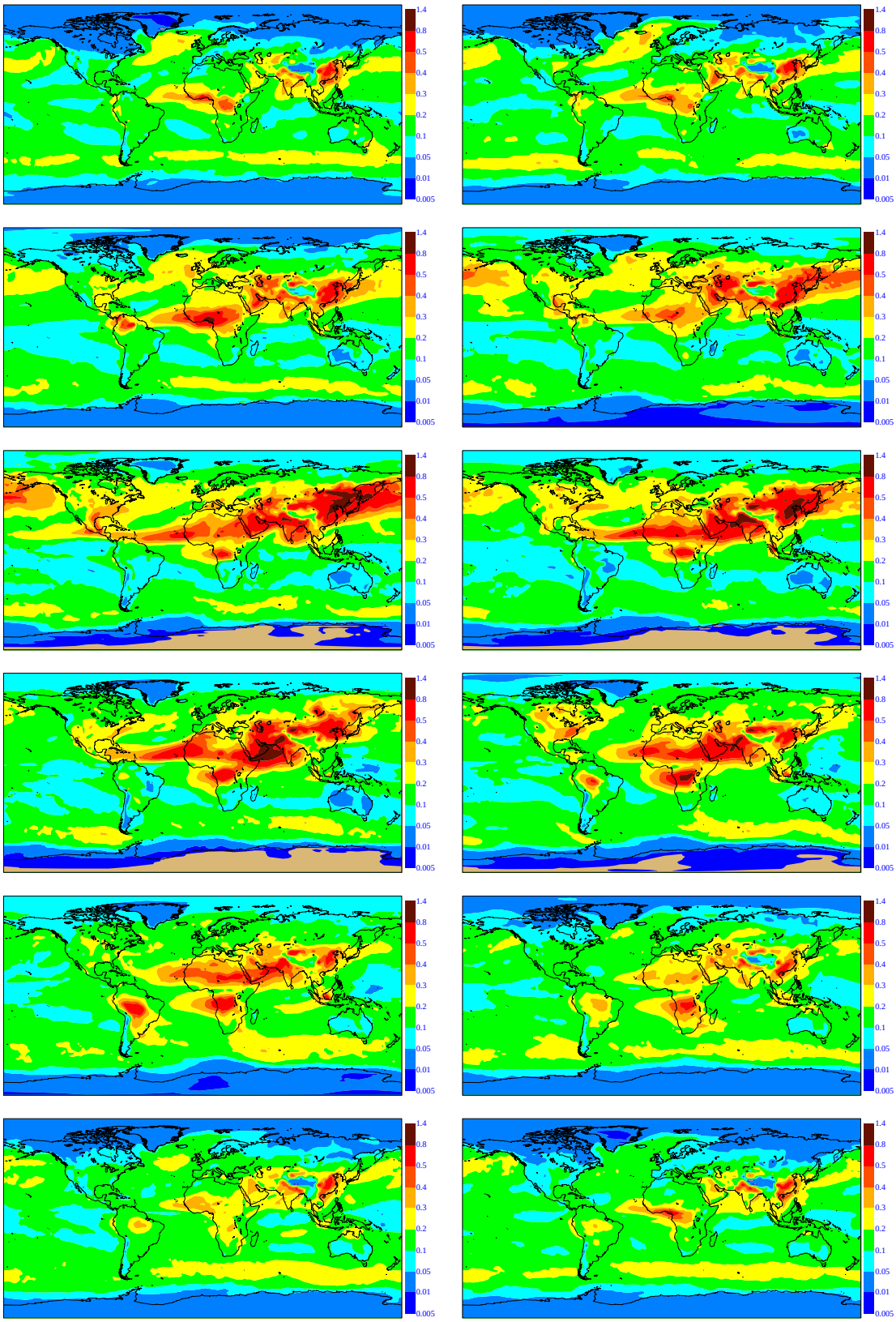

Figure 3: The month-by-month total aerosol optical depth for 2003, from the MACC aerosol reanalysis (see text). January is top left, February is top right, other months follow in a similar way.

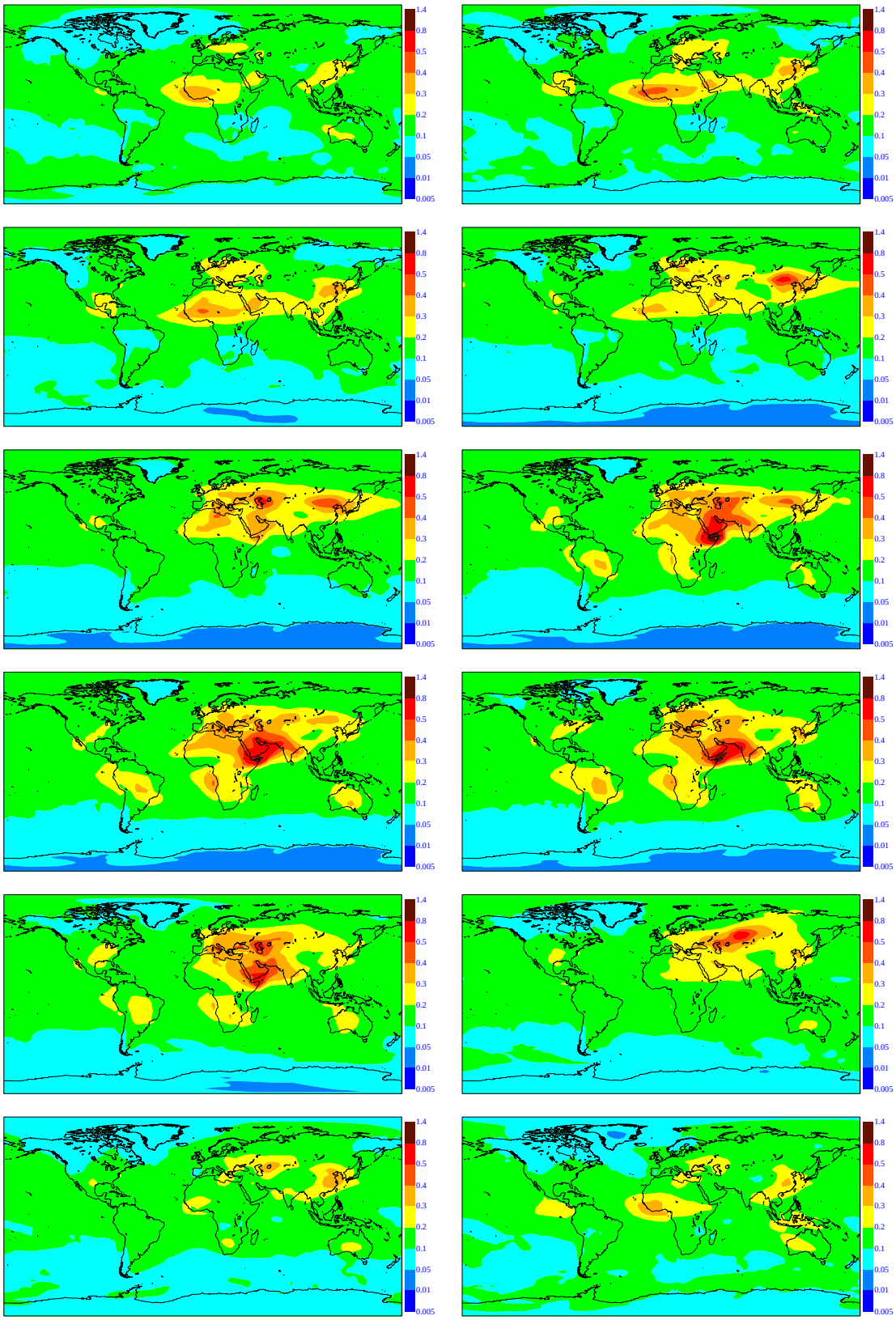

Figure 4: The month-by-month total aerosol optical depth from the operational aerosol climatology, derived from Tegen et al. (1997). January is top left, February is top right, other months follow in a similar way.

3 MACC vs. GEMS

Even without considering changes to the representation of the prognostic aerosols, the two reanalyses differ by the model horizontal resolution and the cycle of the operational library: GEMS was run with T_L159 L60 model, with a grid of $[1.125deg]^2$, and the version 32R3 of the libraries made operational in November 2007, whereas MACC was run with the T_L255 L60 model, a $[0.70deg]^2$ grid and cycle 36R1 of the libraries made operational in January 2010. Between these two cycles, a significant number of changes were made to the model package of physical parametrisations (revised entrainment in the convection scheme, revised melting of falling snow, revised diffusion coefficients in the vertical diffusion scheme, revised turbulent orographic form drag, revised snow scheme, introduction of a non-orographic wave scheme, and revised trace gas climatology). Similarly modifications were brought to the assimilation system and dynamical schemes (conserving interpolation scheme for trajectory fields in 4D-Var). All of the above changes obviously affect the analysis of the standard meteorological fields of pressure, temperature, and wind, which is the background information upon which the analysis of aerosols is performed.

Both the GEMS and MACC systems are based on assimilation of MODIS Aerosol Optical Depth (AOD) at 550nm. However they differ fundamentally in the way the observations constrain the analysis through a different definition of observation errors, and the introduction of a variational bias correction. Changes in the background errors were also made, but those were shown to be minor and went into the direction of de-emphasizing the role of the first-guess in favor of the observations. These changes were introduced because the GEMS reanalysis was shown to be biased with respect the assimilated observations (Benedetti et al, 2008). In-depth investigation showed that this behavior was caused by the assignment of observation errors on MODIS AOD as a percentage of the AOD plus a correction depending on the scattering angle. This definition of errors did not allow the analysis to correct large values of AOD, due to the correspondingly large errors assigned to the observations. A bias in the analysis visible in the global means was the result. The GEMS analysis was shown however to perform well in terms of temporal and spatial variability of the aerosol fields in comparisons with AERONET and other independent datasets (Mangold et al 2011).

The MACC reanalysis was constructed on very different premises. First of all the observation errors were fixed to values of 0.1 over land, and 0.05 over the ocean. Additionally a variational bias correction was implemented based on the operational set-up for assimilated radiances following the developments by Dee and Uppala (2008). The bias model for the MODIS data consists in a global constant which is adjusted variationally in the minimization based on the first-guess departures. Although simple, this bias correction worked well in the sense that the MACC analysis is not biased with respect to the MODIS observations. Moreover this approach has the advantage to be tied to the optimization of the cost function, and as such it is estimated online, not requiring previous pre-processing of the observations. The bias error model allows more complex treatment with the addition of other bias predictors which are relevant for AOD, for example instrument geometry, viewing angle, cloud cover, wind speed etc. Improvements to the bias model and the inclusions of other high-accuracy data sets that can anchor the MODIS bias (for example AODs from a selected list of AERONET stations), will be undertaken in MACC-II (the follow-on project to MACC, covering 2012-2014).

3.1 Monthly mean global fields

As discussed in Benedetti et al. (2009), the aerosol optical depth at 550 nm (hereafter τ_{550}) retrieved from measurements by the MODIS instrument on-board both the Terra and Aqua satellites have been

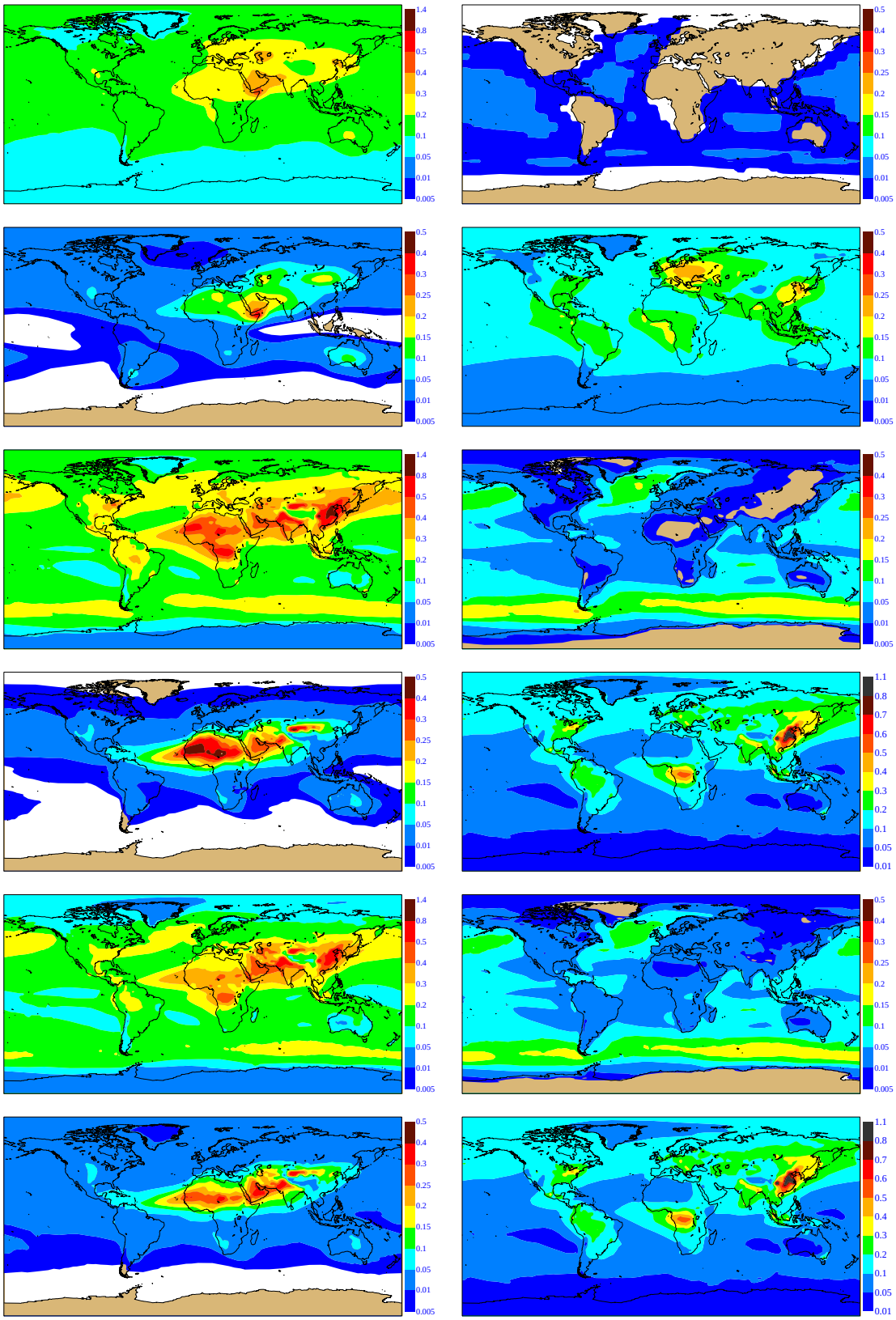

Figure 5: The 2003 mean annual optical depth for total, sea-salt, dust, and anthropogenic aerosols from the operational aerosol climatology (top four panels), the GEMS aerosol reanalysis (middle four panels), anf the MACC aerosol reanalysis (lower four panels).

assimilated to provide an analysis of the aerosol loading in the atmosphere. The profiles of the aerosol mixing ratios for the 11 aerosol types and bins are used to compute a total aerosol optical depth (TAOD). This TAOD is then compared to the observed aerosol optical depth and a variational assimilation modifies the model total aerosol optical depth to make it consistent with the observation, but keeping the profile shapes and distribution between aerosol types provided by the forward model in its trajectory calculations. Figure 1 presents the global distribution of τ_{550} derived from MODIS on Aqua for the 12 months of 2003, whereas Figures 2 and 3 present the equivalent field built from 24-hour forecasts started from the GEMS and MODIS aerosol analyses. Unsurprisingly, there is a general agreement with the MODIS observations, in terms of patterns, but differences can be seen, which are of different origin.

Overall, GEMS τ_{550}^{gems} is higher than MACC τ_{550}^{macc}, for all months. The differences between the two analyses can be explained by different factors. As discussed above, this is linked to the different handling of the bias correction and of the background error in GEMS and MACC where MODIS data are available. GEMS had a bias correction linear with τ_{550} whereas MACC has a fixed one (Benedetti et al., 2008). At high latitudes, in Northern hemisphere (January to April, November and December) in areas where no MODIS observation is available, the higher aerosol loading is propagated from lower latitudes where MODIS observations are available. The GEMS global optical depth is 0.23 whereas it 0.20 for MACC, and this overestimation shows up more prominently in areas with small τ_{550} than in areas with large one, even if the problem in GEMS was rather global.

Then, concentrating on areas at mid- and lower latitudes where MODIS data are not available (Sahara, Saudi Arabia, part of Australia for all months, all areas with high surface albedo for which the aerosol retrieval is not attempted), the GEMS system usually produces larger aerosol amounts than the MACC system. In these potentially dust-rich areas, the smaller aerosol loading in MACC is due to a revision of the dust emission following assessment of the GEMS analysis. However, the revision went too far, and another assessment concentrating on dust (Huneeus et al., 2011) concluded that the MACC dust aerosol amount is now relatively low over the sources regions and that the plumes extending from these regions (e.g., over the Atlantic ocean) are too rich in small particles (radius smaller than 0.5 micron) at the expenses of the bigger particles (radius larger than 1 micron).

Other areas of difference between GEMS and MACC are areas where biomass burning is present at certain times of the year (Amazon Basin, Central Africa, from August to November). Two changes occurred between GEMS and MACC: first, the description of fire emissions moved from GFEDv2 (Global Fire Emission Dataset, version 2) to GFEDv3.0, with overall 22 percent smaller emissions in the newer database (van der Werf, 2010), and the emissions redistributed according to the MODIS daily Fire Radiative Power.

Finally, the areas rich in sulphate-based aerosols (e.g., China) also underwent a change as a bug in the conversion from SO_2 to SO_4 in GEMS was corrected for MACC, bringing an overall decrease and therefore more realistic values for sulphate aerosols.

3.2 Comparison with climatology and other satellite-based aerosol products

Figure 4 presents for the 12 months of the year the climatology for the aerosol optical depth, which has been in use in the ECMWF operational system since October 2003. It is based on the climatological distribution of sea salt, dust, organic and black carbon, and sulphate aerosols, compiled by Tegen et al. (1997). Comparison between Figure 4 and either Figure 2 or 3 shows that this climatology is deficient on several accounts. The climatological τ_{550}^{C} is missing the large aerosol loading over China over most of the year, the maximum in aerosol loading linked to the biomass burning over South America while

present is too weak and occurs too early in the year. A similar situation prevails for the aerosol linked to biomass burning in Central Africa. On the other hand, τ^C_{550} shows a maximum near the Horn of Africa from June to September, which is more diffuse and over a wider area in the MODIS observations (Fig.1) and the GEMS and MACC analyses (Figs. 2 and 3).

Figure 5 compares, on an annual mean basis, the total, sea-salt, dust, and anthropogenic aerosols, from the climatology (top four panels), the GEMS (middle four panels) and MACC analyses (bottom four panels). The differences in amplitude and geographical distribution of the optical depth of these three basic aerosol types are confirmed. The sea salt aerosols are underestimated over the oceans of both the Northern and Southern hemispheres, the dust aerosols over the desert areas of Sahara, Pakistan/Rajasthan and Taklamakan are underestimated. The aerosols of anthropic origin over China and the foothills of the Himalayas are underestimated as is the outflow over the North Pacific. On the contrary, too much anthropogenic aerosols are present in the climatology over Europe, west of Central America and over the oceanic areas of South-East Asia/Tropical West Pacific.

Figure 6 presents the monthly aerosol optical depth at 555 nm for 2003 derived from MISR (the Multi-angle Imaging Spectroradiometer on-board the Terra satellite). There is a good agreement with the global distribution and values given by MODIS. Interestingly, the multi-angle approach allows MISR to provide aerosol optical depth over the desert-like bright surfaces that MODIS cannot handle. Whereas there is not an absolute one-to-one correspondence between the MODIS and MISR aerosol fields, the agreement is remarkable, and provide an a-posteriori justification for using MODIS aerosol observations in the GEMS/MACC aerosol system. This is not the case with the aerosol optical depth derived from MERIS (the Medium-resolution Imaging Spectroradiometer, on-board the Envisat satellite). (NB: The MERIS data were downloaded from the current (October 2011) version of the NASA Giovanni web site). For the same months in 2003, Figure 7 shows prevalent high values of τ_{550} for most of the year over South America, Central Africa. No retrieved τ_{550} is provided for a large fraction of the Eurasian continent, North America, Australia and South Africa.

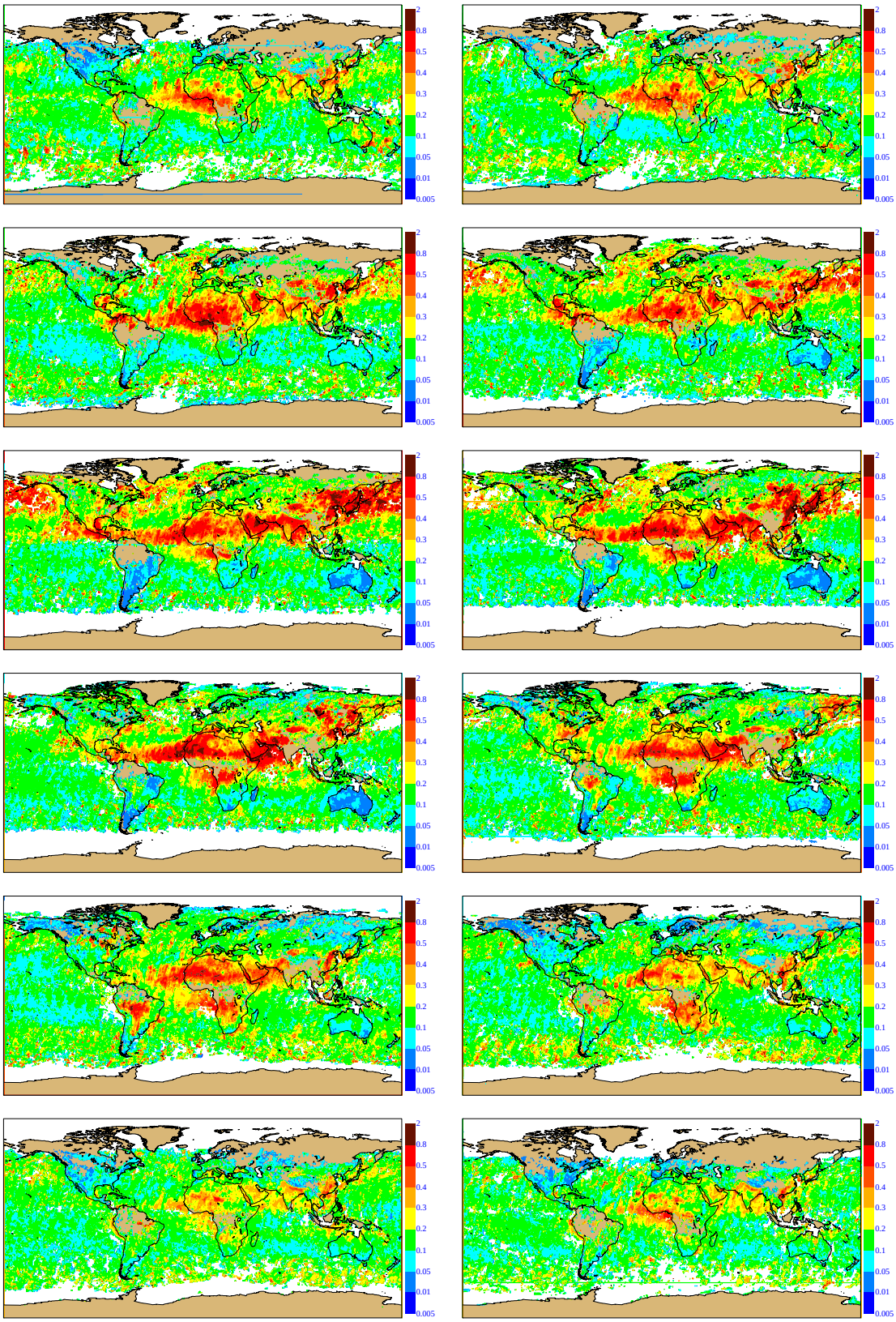

Figure 6: The month-by-month total aerosol optical depth derived from the MISR spectroradiometer on the Terra satellite. January is top left, February is top right, other months follow in a similar way.

3.3 Comparison with ground-station aerosol measurements

In the following, the various changes discussed in section 3.1 can also be seen in comparison with surface observations. The aerosol optical depth produced by the GEMS and MACC systems are compared with the aerosol optical depth at 500 nm τ^A_{500} derived from radiometric measurements at AERONET (AErosol RObotic NETwork) stations (Holben et al., 1998, Dubovik et al., 2002). The GEMS and MACC values are produced by the respective models starting from the relevant analyses at 00 UTC during the first 24 hours of individual forecasts. Table 1 presents the list of the AERONET stations providing measurements during 2003, sampled in such a way that a/ data for all seasons are available, b/ selected stations are at least 250 km apart from each other, and c/ for each month, a dominant aerosol type can be defined.

Figures 8 and 9 present the comparison for four stations where maritime aerosols are likely to be prevalent (Amsterdam Island, Ascension Island, Nauru, and Tahiti). Eight sites with dust aerosols are then shown in Figures 10 to 13 (Fig.10: Banizoumbou, Capo Verde; Fig.11: Dahkla, Dalanzadgad; Fig.12: Ilorin, Ouagadougou; Fig.13: Sede Boker, Solar Village). Biomass burning occurs during the year over the four sites presented in Figures 14 (Abracos Hill, Belterra) and 15 (Mongu, Skukuza). Eight sites dominated by anthropogenic aerosols (either black carbon, organic carbon, sulphate or a mix of these) are then presented: Beijing and GSFC in Figure 16, Kanpur and Mexico City in Figure 17, Moscow and Sao Paulo in Figure 18, and Shirahama and Tomsk in Figure 19. For three out of four oceanic stations (Figs. 8 and 9), there is relatively little change between GEMS and MACC for Amsterdam Island, Ascension Island and Tahiti, which are all located in the Southern hemisphere, rather away from the Intertropical Convergence Zone and all getting a good coverage of MODIS observations. On the other hand, Nauru (four top panels in Fig. 9) is within the ITCZ, gets many more cloudy to overcast days and a more limited coverage by MODIS observations. In January and April, the beginning of the month is devoid of MODIS observations and τ_{550} reflects more heavily the model-driven aerosols. There is a sizeable difference in model τ_{550} likely to be linked to changes in the surface wind (used to diagnose the surface emission of sea salt particles) as part of the changes to the model physics package between the two analyses.

The next eight stations with dust likely to be the dominant aerosol type fall into two categories, those with (Capo Verde, Dahkla, Dalanzadgad, Ilorin, Ouagadougou) or without (or very few) MODIS observations (Banizoumbou, Sede Boker, Solar Village). When MODIS observations are available, the MACC τ_{550} is generally in better agreement with AERONET observations if those are available. When no MODIS data is available, τ^{gems}_{550} is generally larger than τ^{macc}_{550} (Banizoumbou, Ouagadougou in April, Sede Boker), reflecting the reduction in dust emission over the Sahara between GEMS and MACC. For stations less or not connected with Saharan emissions (Sede Boker, Solar Village, Dalanzadgad), the model τ_{550} appears to be larger than τ^A_{500}. Interestingly, there is a discrepancy between MODIS τ_{550} and τ^A_{500} in Dalanzadgad for three out of the four months shown, possibly due to some limitation in the MODIS retrieval of aerosol optical depth over the middle-bright surfaces of Mongolia.

Stations in biomass burning areas of South America (Abracos Hill and Belterra, in Fig. 13) and of Central/South Africa (Mongu and Skukuza, in Fig. 14) usually show slightly smaller τ^{macc}_{550} compared to τ^{gems}_{550} with a generally better agreement of τ^{macc}_{550} with MODIS τ^M_{550}. However, there are also instances with huge AERONET τ^A_{500}, which are not well captured by the analysis system (Abracos Hill and Mongu, in July and October 2003).

For the remaining six stations where anthropogenic (organic and black carbon, sulphate aerosols) are dominant, τ^{macc}_{550} is generally smaller than τ^{gems}_{550}, particularly when MODIS observations are not available (Moscow in January and November 2003, Tomsk in January 2003). Otherwise, as over other stations, the agreement between τ^{macc}_{550} and MODIS τ^M_{550} is better than between τ^{gems}_{550} and MODIS τ^M_{550}.

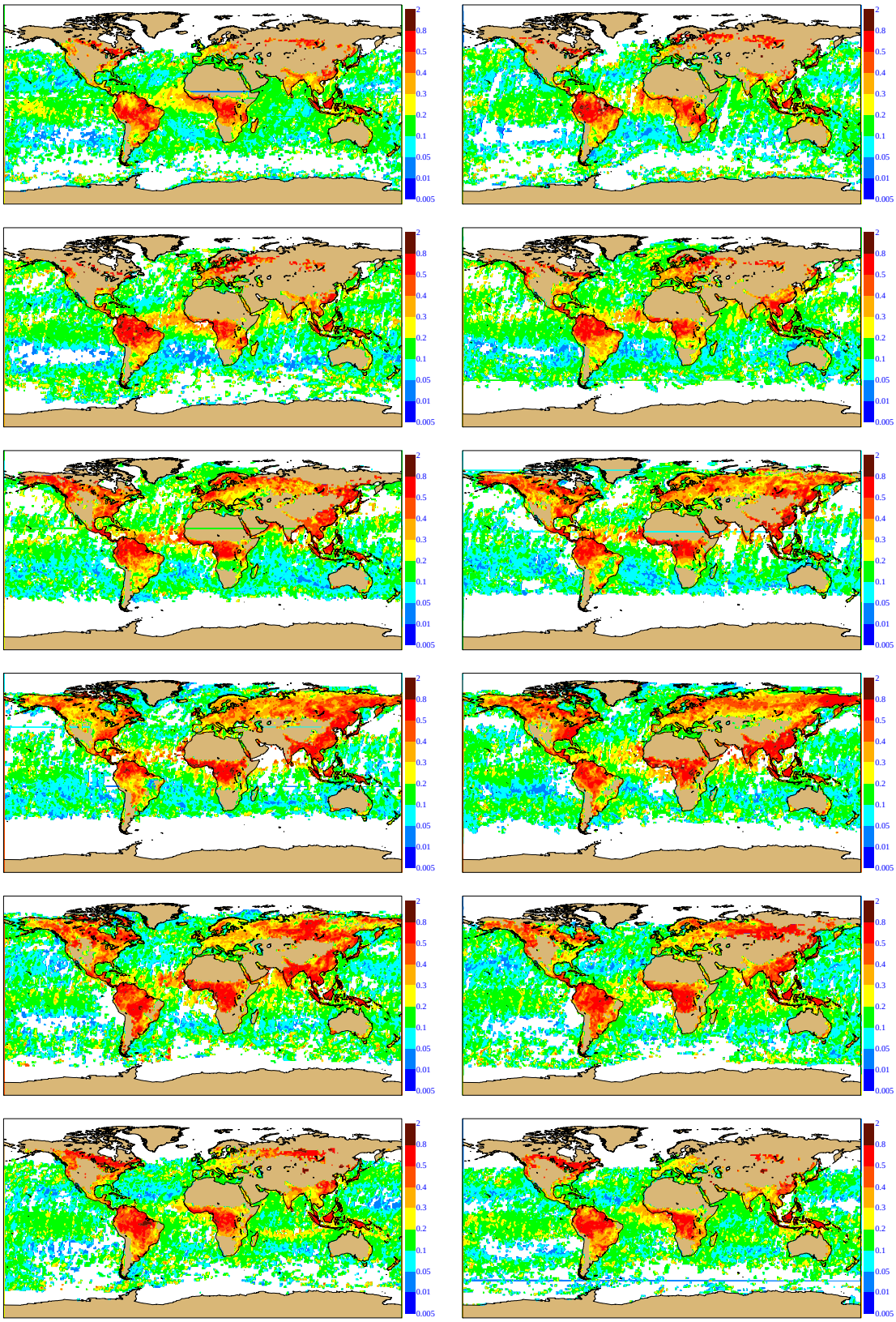

Figure 7: The month-by-month total aerosol optical depth derived from the MERIS spectroradiometer on the Envisat satellite. January is top left, February is top right, other months follow in a similar way.

Table 2 presents for the same months and same stations the bias and root mean square error between the AERONET τ_{500} and the GEMS and MACC values during the first 24 hours of the forecasts starting from the relevant analyses at 00 UTC. In this Table, *Nstat* is not the number of AERONET observations used in the calculation of the corresponding bias and root mean square error (rmse), but the number of forecast-observation differences. This number will be less than or equal to the number of AERONET observations used because the observations are first time-meaned into the same six-hour windows as the forecast data are retrieved. *Nstat* therefore shows how many six-hour windows AERONET data existed in. A row of dashes means there was no AERONET data at all for that site in that month. Note also that AERONET observations are absent in Banizoumbou, Beijing, Capo Verde, Ouagadougou, and Shirihama, so these stations are absent from Table 2.

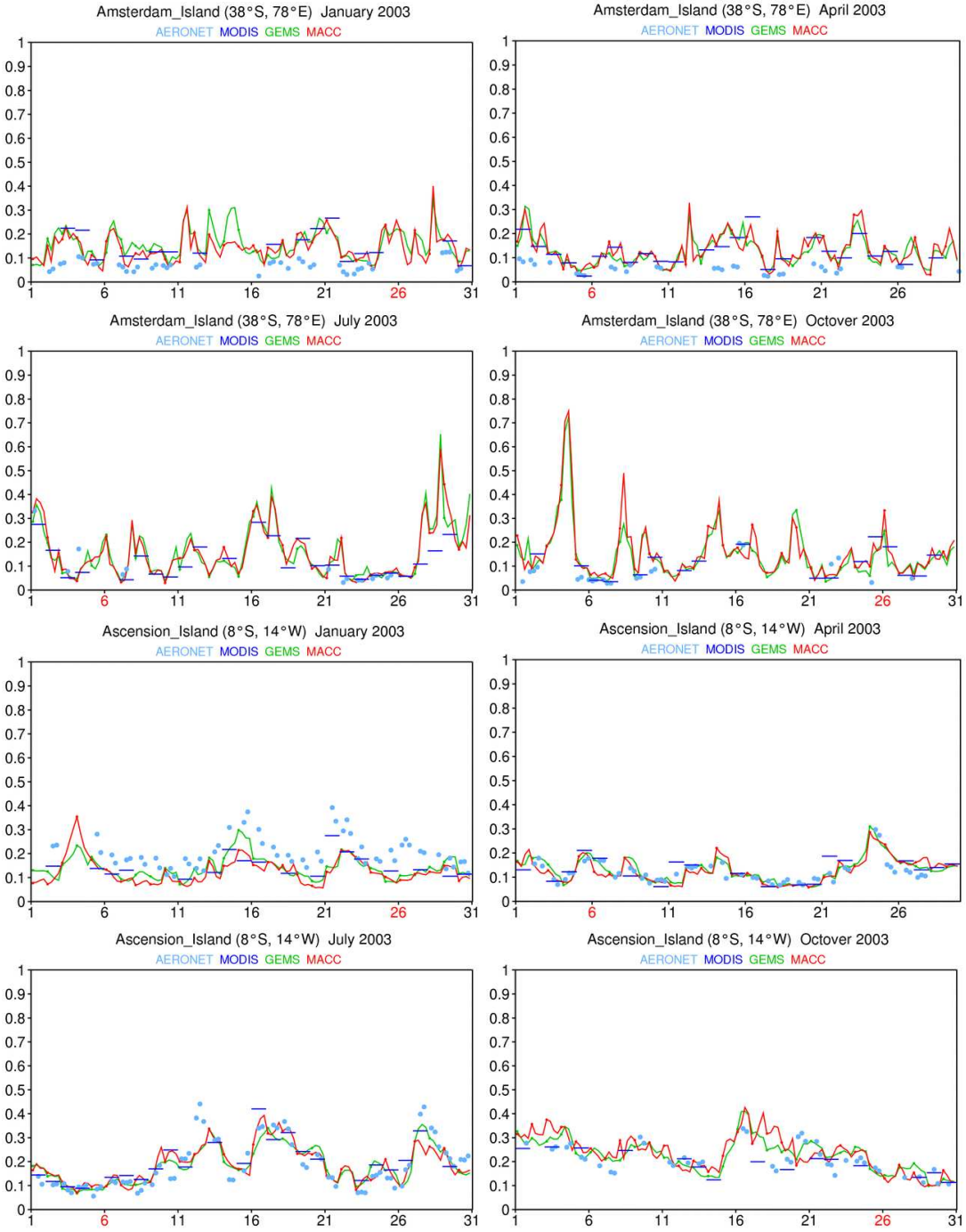

Figure 8: The time-series of aerosol optical depth at Amsterdam Island (top four panels) and Ascension Island (bottom four panels). GEMS (yellow line), MACC (red line) and MODIS (dark blue segment) are observed at 550 nm, AERONET (blue dots) are observed at 500 nm. For each station, the four panels are January (top left), April (top right), July (bottom left) and October (bottom right).

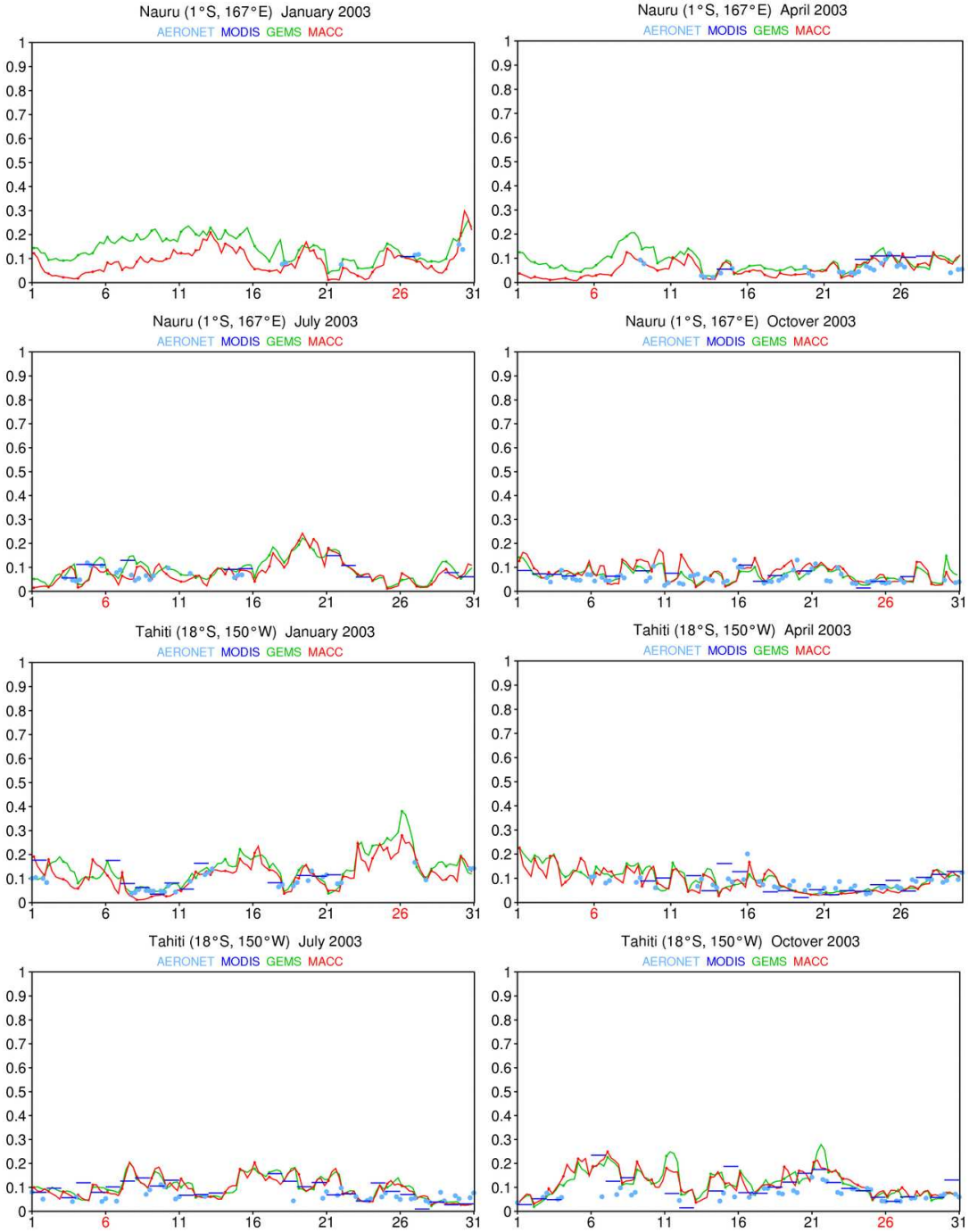

Figure 9: As in Figure 8, but for the island stations of Nauru (top four panels) and Tahiti (bottom four panels).

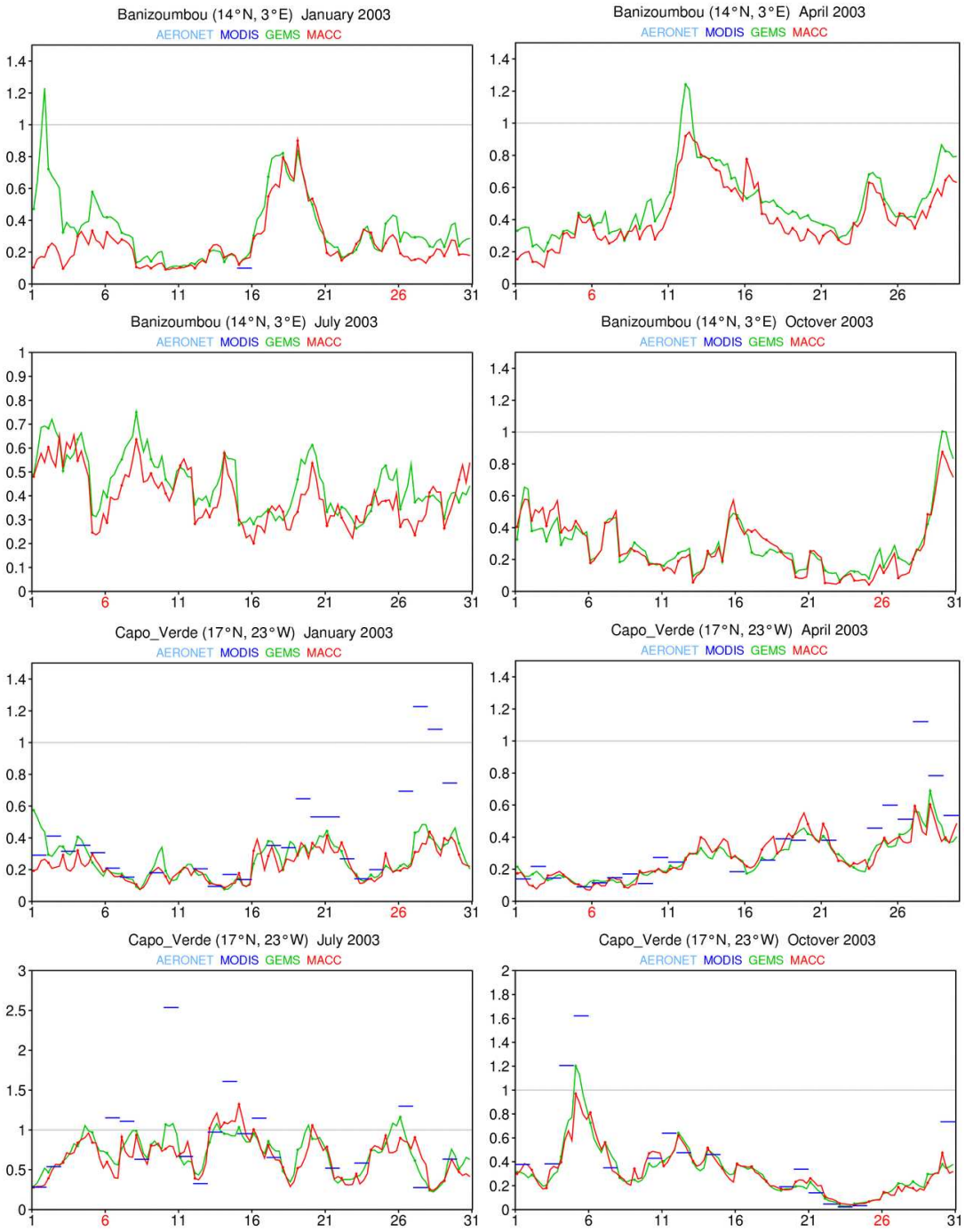

Figure 10: As in Figure 8, but for the stations of Banizoumbou (top four panels) and Capo Verde (bottom four panels).

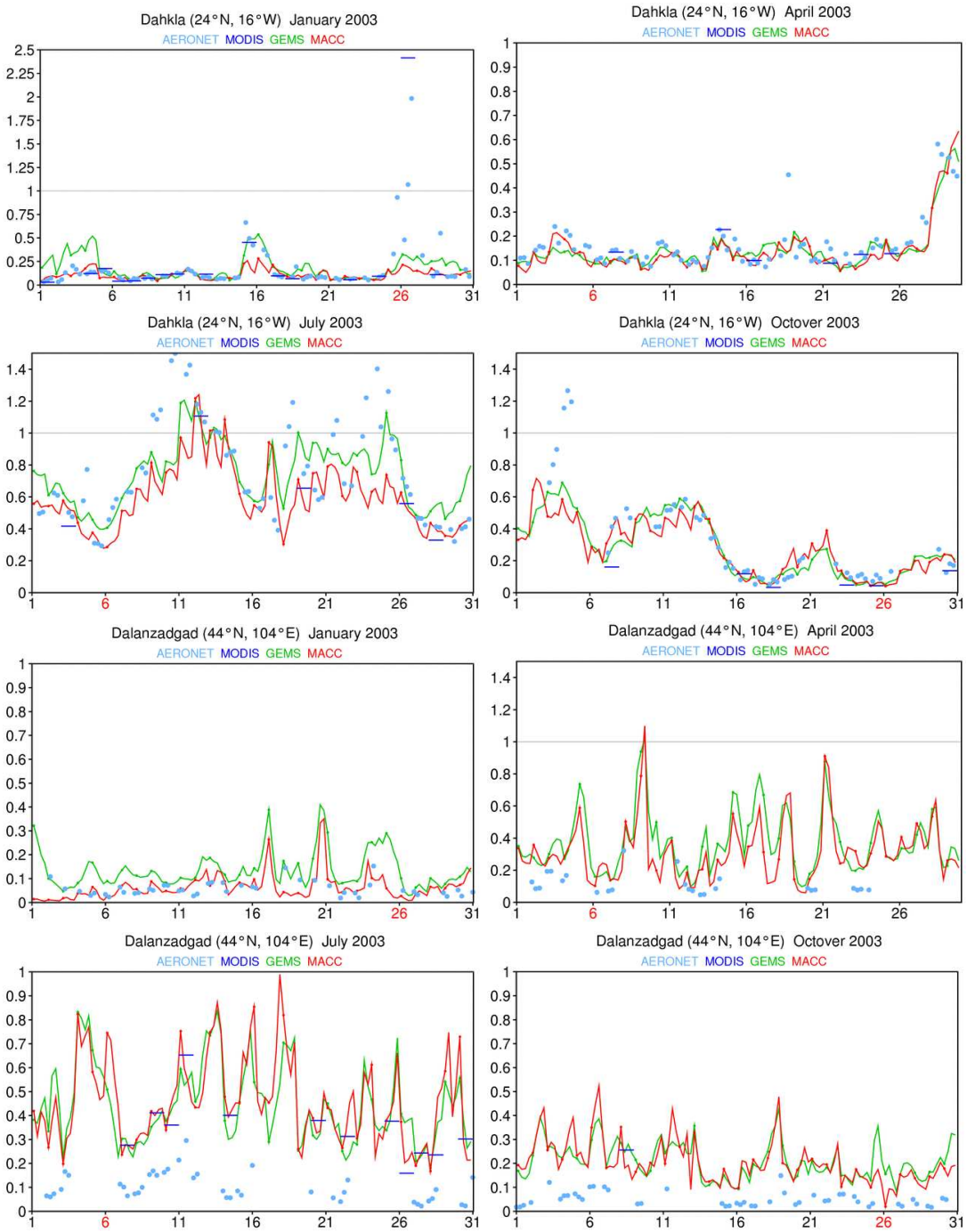

Figure 11: As in Figure 8, but for the stations of Dahkla (top four panels) and Dalanzadgad (bottom four panels).

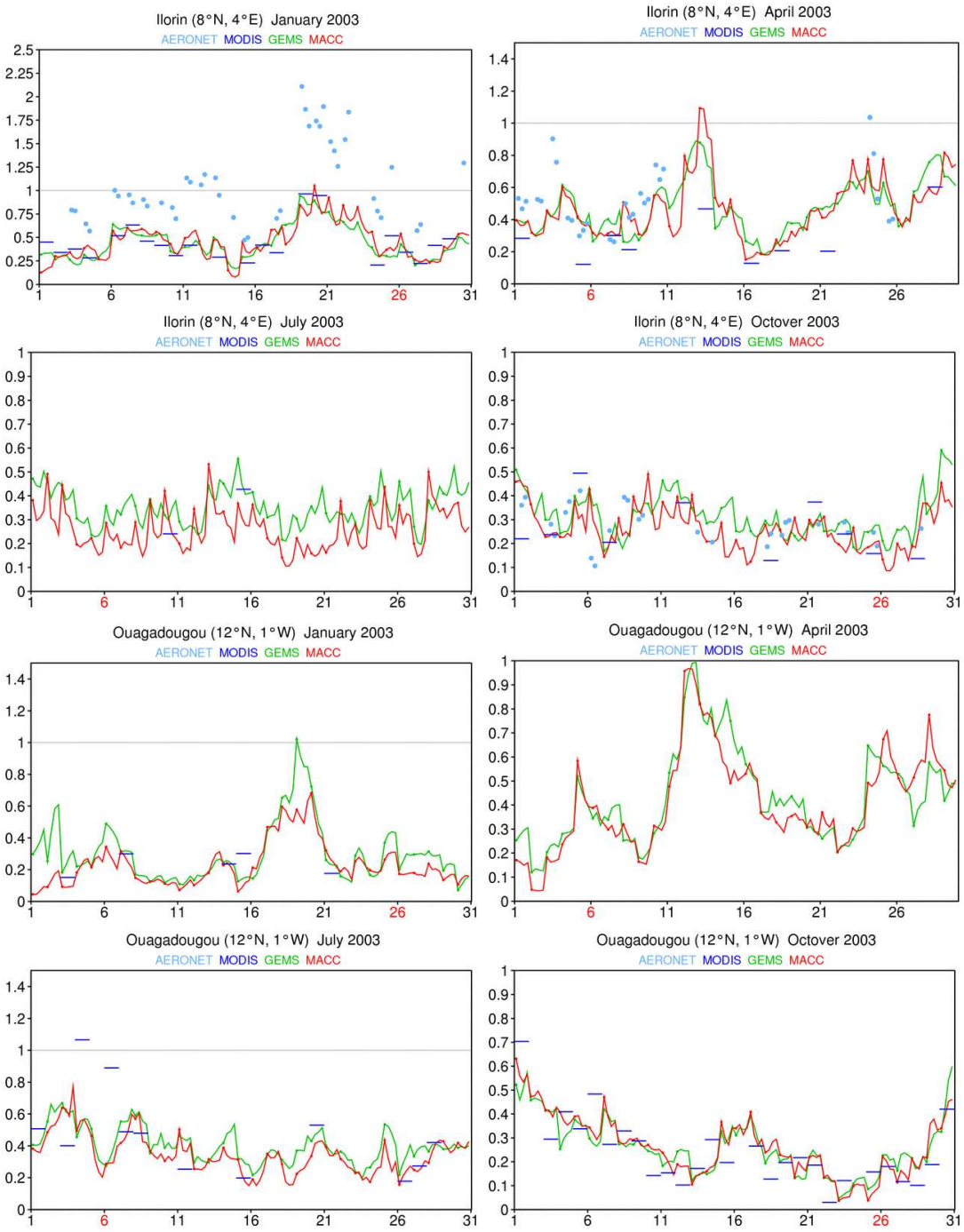

Figure 12: As in Figure 8, but for the stations of Ilorin (top four panels) and Ouagadougou (bottom four panels).

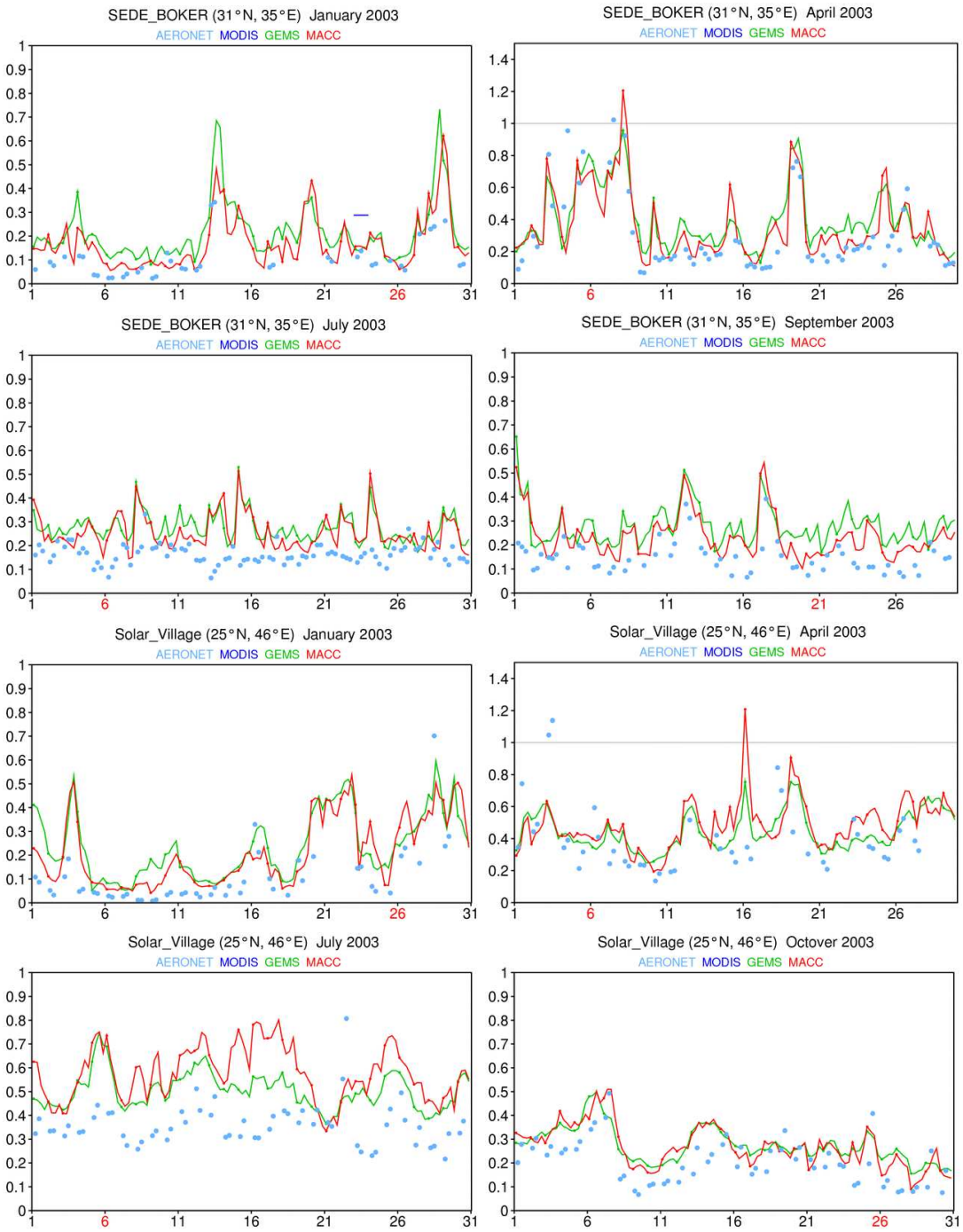

Figure 13: As in Figure 8, but for the stations of Sede Boker (top four panels) and Solar Village (bottom four panels). Note that the fourth month at Sede Boker is for September.

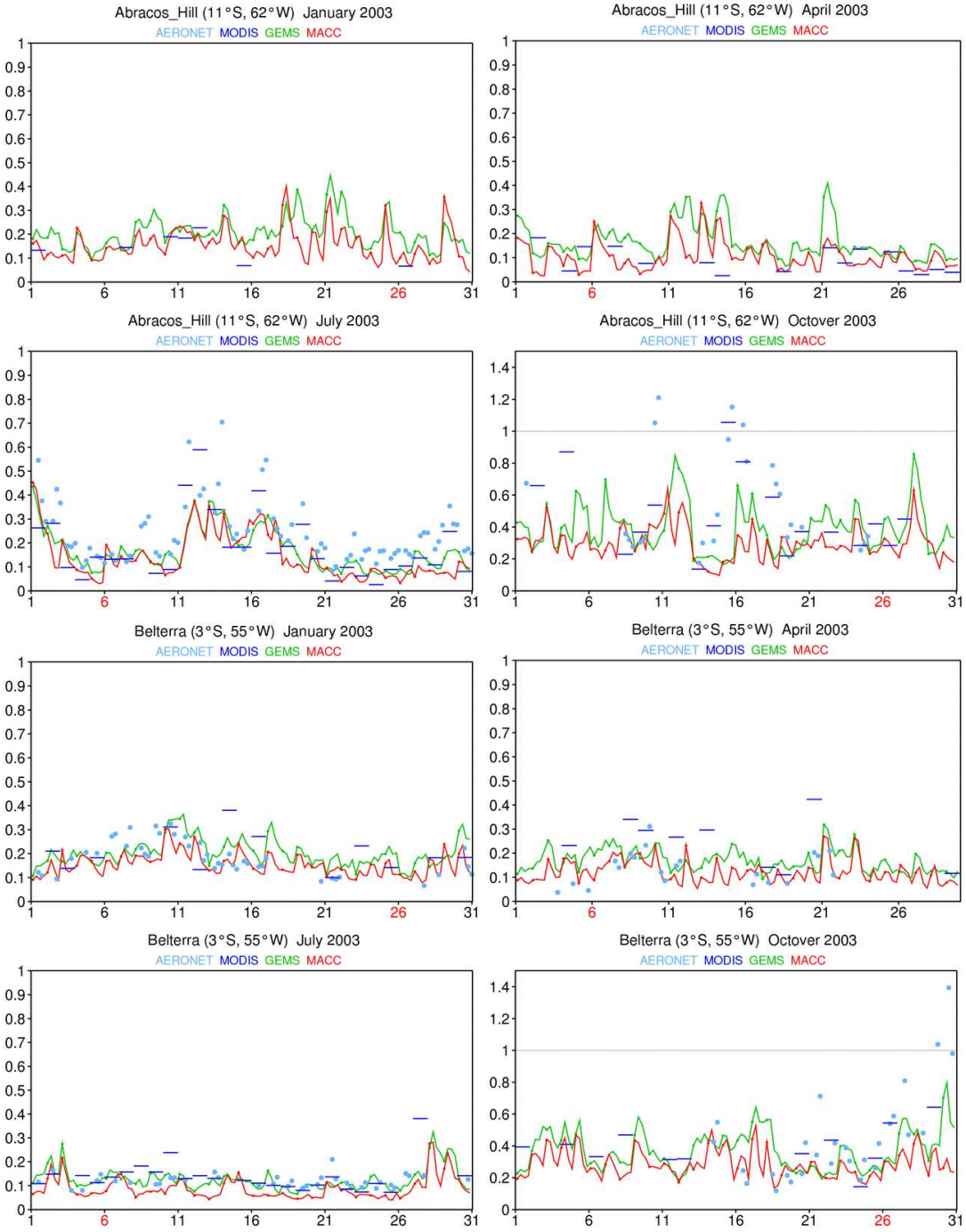

Figure 14: As in Figure 8, but for the stations of Abracos Hill (top four panels) and Belterra (bottom four panels).

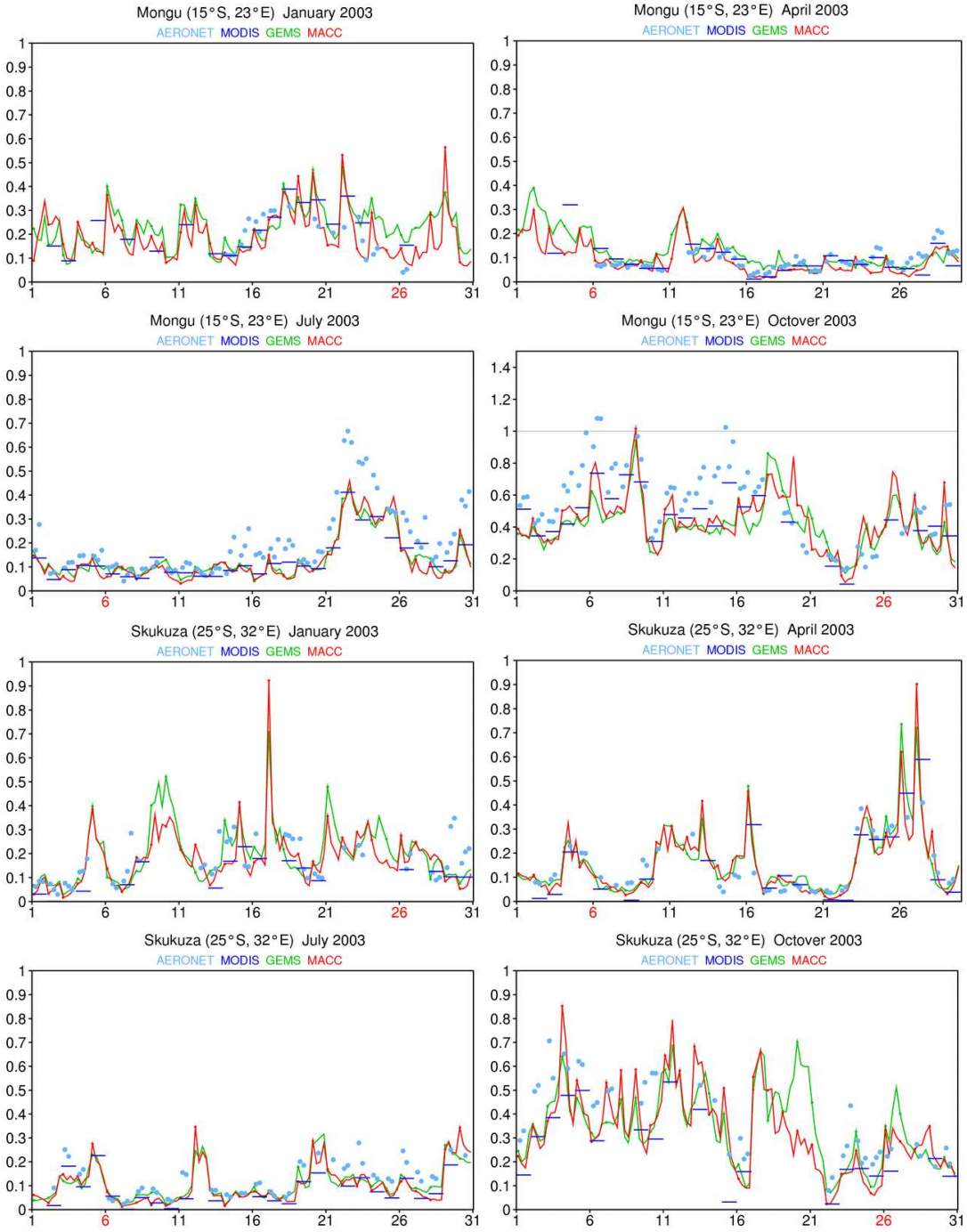

Figure 15: As in Figure 8, but for the stations of Mongu (top four panels) and Skukuza (bottom four panels).

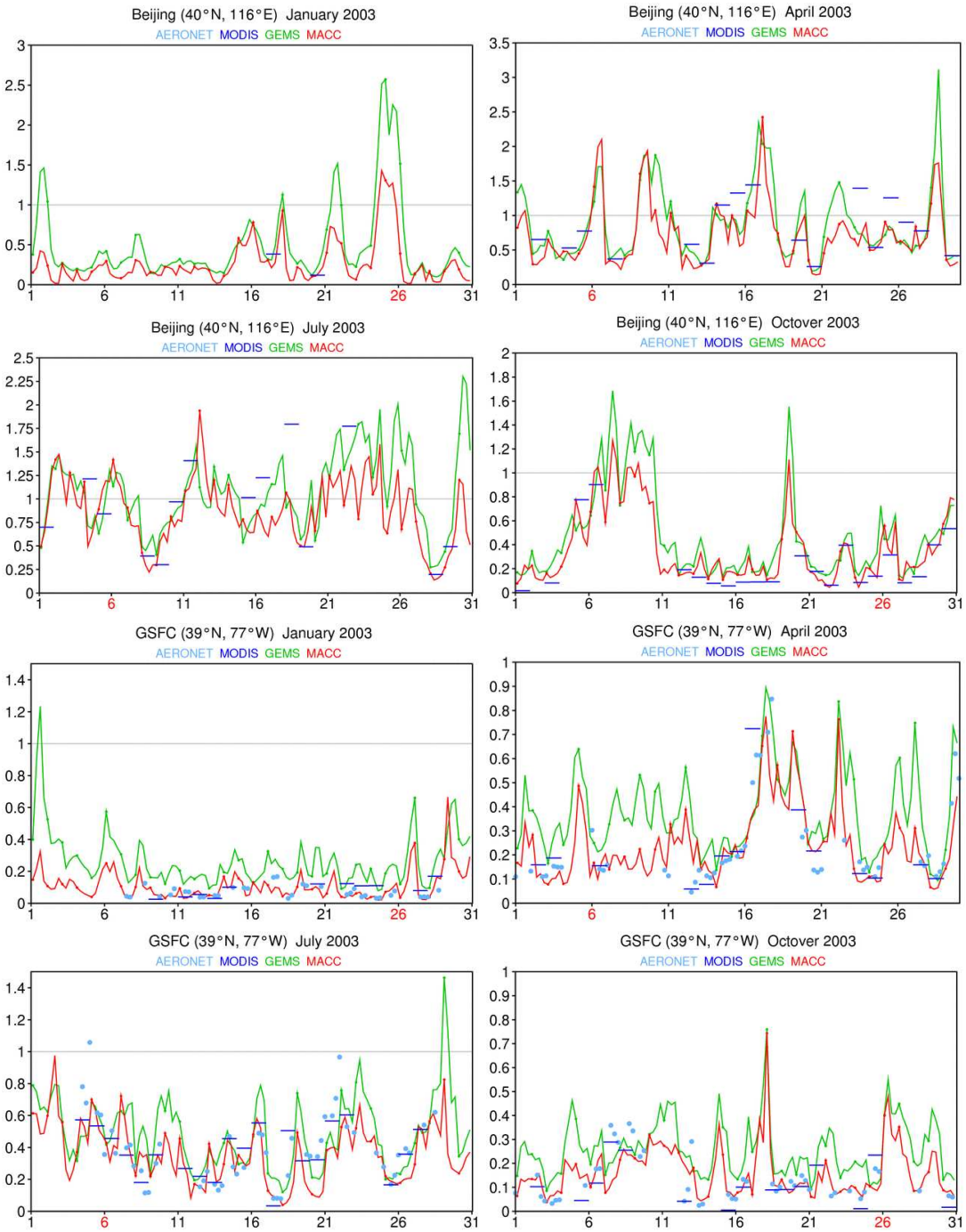

Figure 16: As in Figure 8, but for the stations of Beijing (top four panels) and Goddard Space Flight Center (GSFC) (bottom four panels).

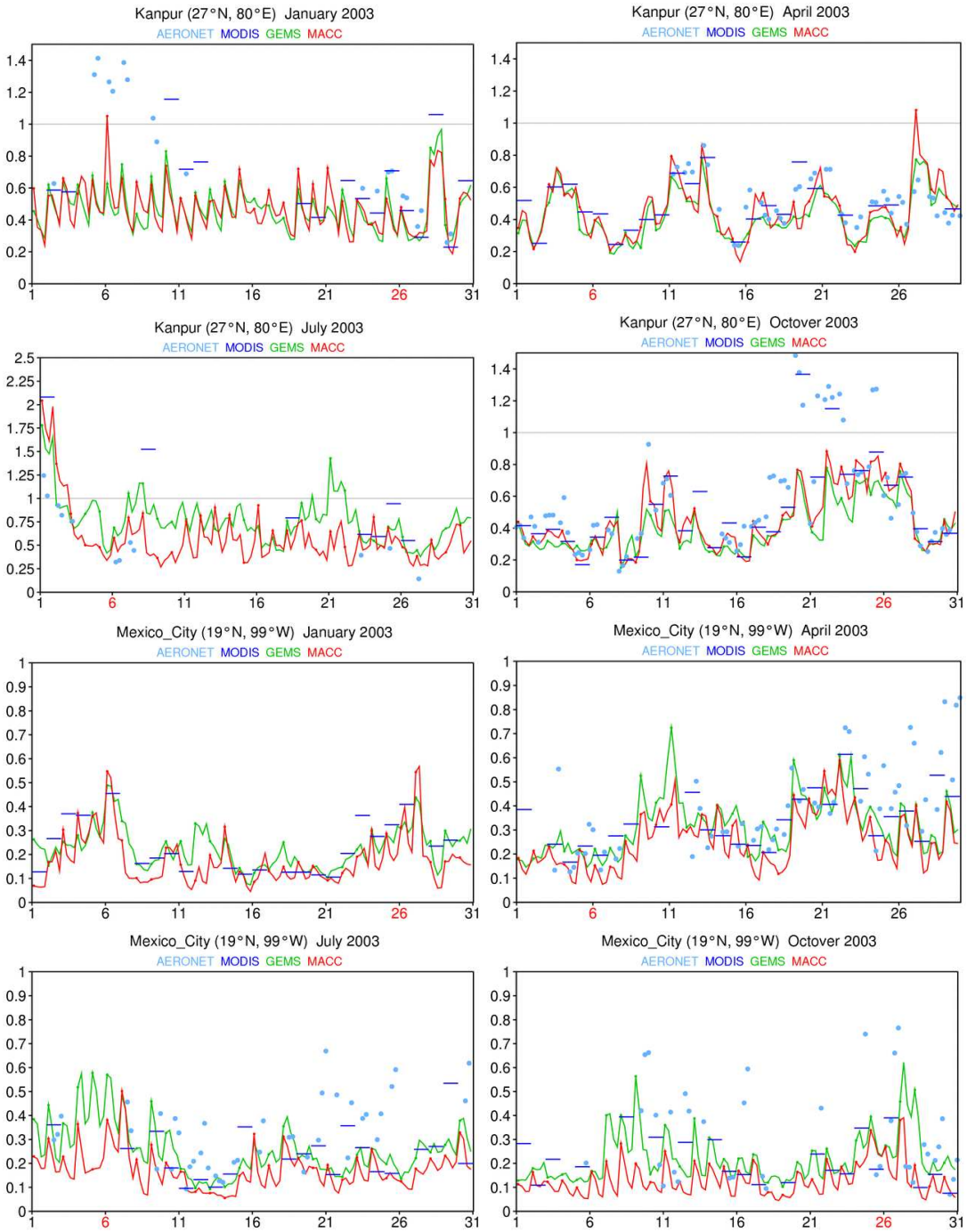

Figure 17: As in Figure 8, but for the stations of Kanpur (top four panels) and Mexico City (bottom four panels).

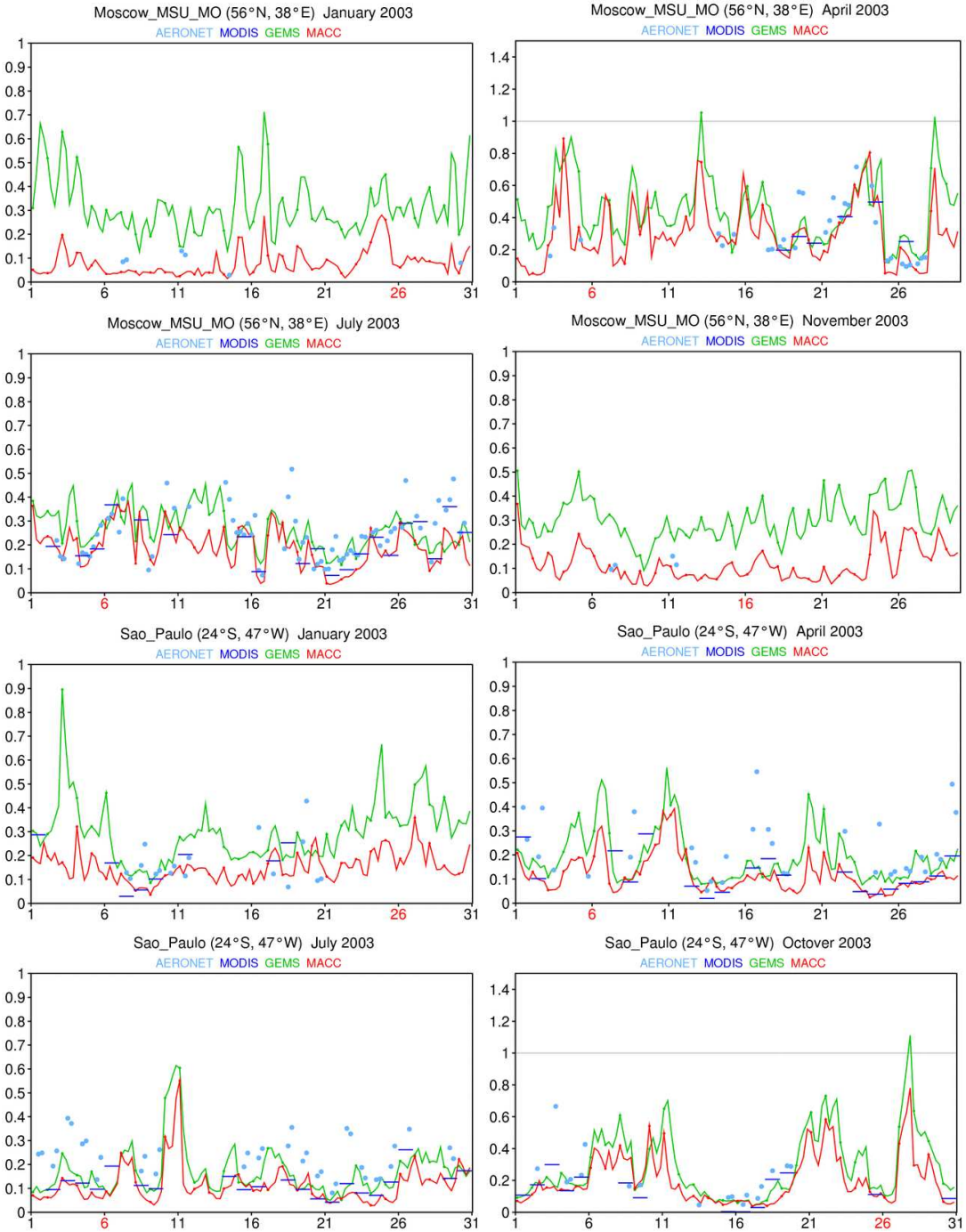

Figure 18: As in Figure 8, but for the stations of Moscow (top four panels) and Sao Paulo (bottom four panels). Note that the fourth month at Moscow is for November.

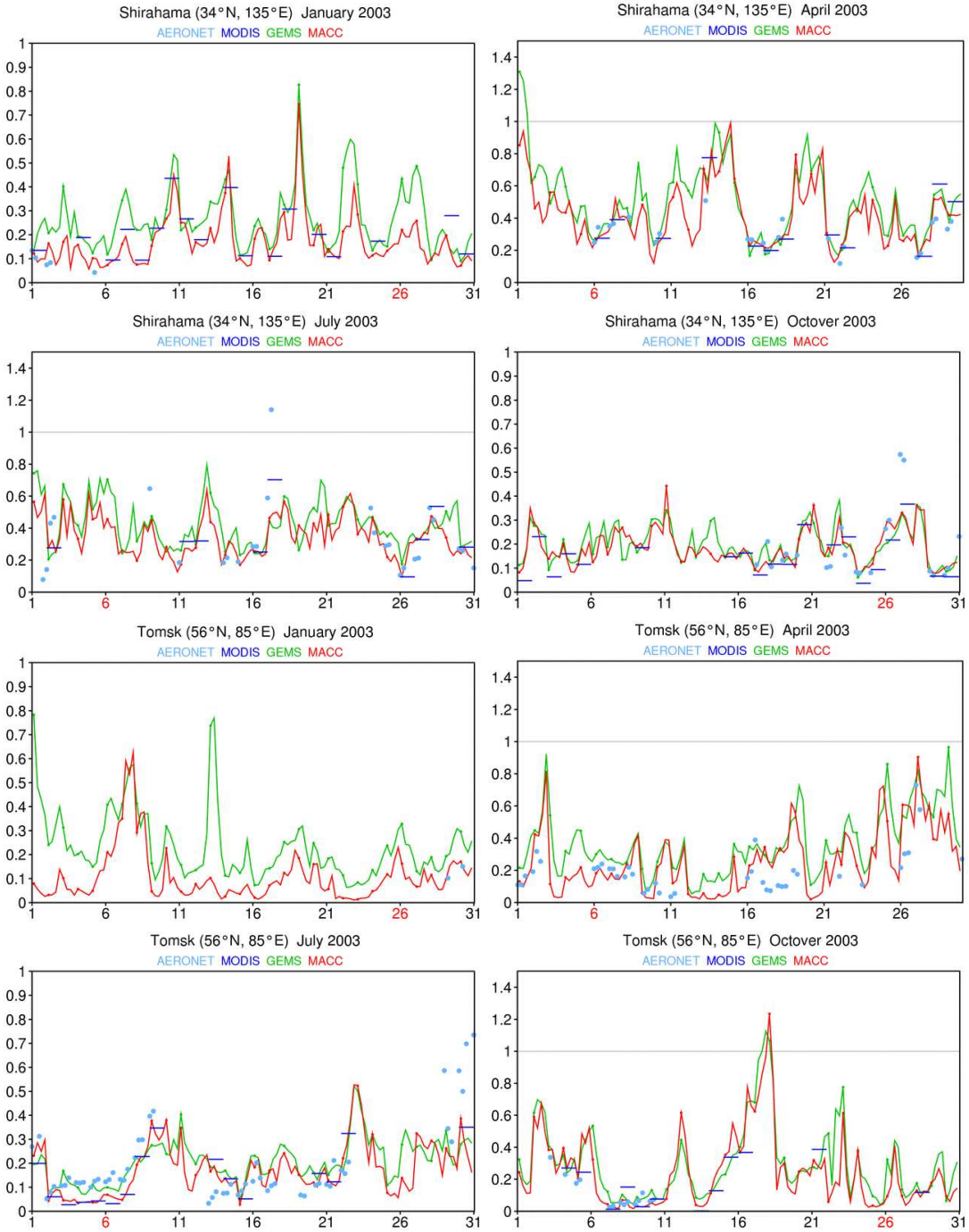

Figure 19: As in Figure 8, but for the stations of Shirahama (top four panels) and Tomsk (bottom four panels).

Station name	ID	Latitude	Longitude	Dominant process Aerosol origin	Months considered
Abracos Hill	ABH	10.76 S	62.36 W	biomass burning	01 04 07 10
Amsterdam Island	AMI	37.81 S	77.57 E	maritime	01 04 07 10
Ascension Island	ASI	7.98 S	14.41 W	maritime	01 04 07 10
Banizoumbou	BAN	13.54 N	2.67 E	dust	01 04 07 10
Beijing	BEJ	39.98 N	116.38 E	anthropogenic	01 04 07 10
Belterra	BET	2.65 S	54.95 W	biomass burning	01 04 07 10
Capo Verde	CVR	16.73 N	22.93 W	dust	01 04 07 10
Dahkla	DAK	23.72 N	15.95 W	dust	01 04 07 10
Dalanzadgad	DAZ	43.58 N	104.42 E	dust	01 04 07 10
GSFC	GSF	38.99 N	76.84 W	anthropogenic	01 04 07 10
Ilorin	ILO	8.32 N	4.34 E	dust	01 04 07 10
Kanpur	KAN	26.51 N	80.23 E	anthropogenic	01 04 07 10
Mexico City	MEX	19.33 N	99.18 W	anthropogenic	01 04 07 10
Mongu	MON	15.25 S	23.15 E	biomass burning	01 04 07 10
Moscow MSU MO	MSU	55.70 N	37.51 E	anthropogenic	01 04 07 11
Nauru	NAU	0.52 S	166.92 E	maritime	01 04 07 10
Ouagadougou	OUA	12.20 N	1.40 W	dust	01 04 07 10
Sao Paulo	SAO	23.56 S	46.73 W	anthropogenic	01 04 07 10
Sede Boker	SBO	30.86 N	34.78 E	dust	01 04 07 09
Shirahama	SHI	33.69 N	135.36 E	anthropogenic	01 04 07 10
Skukuza	SKU	24.99 S	31.59 E	anthropogenic	01 04 07 10
Solar Village	SVI	24.91 N	46.40 E	dust	01 04 07 10
Tahiti	TAH	17.58 S	149.61 W	maritime	01 04 07 10
Tomsk	TOM	56.48 N	85.05 E	anthropogenic	01 04 07 10

Table 1: The names and geographical coordinates of the AERONET stations used for point verification of the aerosol optical depth. All stations are compared in terms of time-series for the months of January, April, July and October 2003, except where noted (Moscow, Sede Boker)

The results in Table 2 are rather mixed. The improvement from GEMS to MACC is rather patchy. The improvement appears more likely for January, whereas deterioration of the results is prevalent at most stations in July. April and October. There are only a few stations where an improvement is seen for most months (GSFC, Sede Boker, Tomsk). Some stations show a systematic deterioration (Belterra, Dahkla, Sao Paulo). Mixed results, usually corresponding to small fluctuations in bias and rmse, are seen in Amsterdam Island, Ascension Island, Kanpur, Nauru, Skukuza, Tahiti). Dalanzadgad shows an improvement betweem GEMS and MACC, but with a bias remaining rather large in April, July and October).

To conclude this comparison with AERONET observations, the analysis system is quite successful at reproducing the temporal variability of the aerosol loading over most stations, whatever the dominant aerosol type. There is certainly space for improvement, likely to come from refinements in the aerosol modelling in the forward model used in the analysis, but also from including other observations in the aerosol analysis system (either τ at other wavelengths or information on the Ångström exponent, which could discriminate between larger vs. smaller aerosol particles and/or absorbing vs. non-absorbing aerosols.

4 Conclusions and perspectives

Despite improvements in the overall Integrated Forecasting System, the aerosol results with the MACC aerosol system are not markedly better than those with the GEMS aerosol system. With MACC, the aerosol analysis system has improved in terms of the definition of the observation errors. Direct result of that improvement is the usually better agreement between τ_{550}^{macc}, the MACC aerosol optical depth, and τ_{550}, the assimilated MODIS optical depth, relative to the agreement between τ_{550}^{gems}, the GEMS aerosol optical depth, and τ_{550}.

As mentioned in section 3, the MACC analysis was designed to be unbiased with respect to the MODIS observations. In view of this, it is not surprising that for some stations the agreement between the MACC reanalysis and the AERONET AOD has not improved. Very often those are stations close to high-albedo areas where the MODIS instrument is known to perform poorly as far as aerosol detection (Ilorin in January and April, Dahkla in July, Dalanzadgad in July and October, to mention a few), or in highly-polluted urban areas (i.e. Sao Paulo in April and July, Mexico City at the end of April and end of July). However, this raises both the question of the de-biasing of the input observations (see Shi et al 2011), and that of using the best-suited datasets for reanalysis purposes, with MODIS remaining one of the longest established, most consistent and highest quality global datasets currently available. In MACC-II the question of assimilating datasets other than the standard MODIS product, especially over high-albedo surfaces, will be addressed.

In areas where MODIS observations are not ingested or are not available, the analysis relies almost exclusively on the forward model. To improve the aerosols over areas with high surface albedo where dust is prevalent, and where MACC has clearly not improved on GEMS, the future system will have to include one or more of the following developments: either a better representation of the dust sources, and/or the use of observations such as MODIS Deep Blue or OMI absorption optical depth, in order to constrain the amount of dust emitted in these areas.

The analysis system has also been upgraded and the added flexibility in accepting satellite observations other than MODIS's and the possibility of analyzing both the total and fine mode optical depth (over the ocean at least) is likely to further the quality of the aerosol analysis.

The representation of the emissions of aerosols linked to fire activity has received considerable attention. In the comparisons carried in this paper, the biomass burning emissions are taken from two versions of the GFED, over the period 2003-2008. For 2009 and 2010, MACC uses the more recent GFAS (Kaiser et al., 2011), which is not addressed here.

Stn. ID	JAN Nstat	Bias GEMS	Bias MACC	rmse GEMS	rmse MACC	APR Nstat	Bias GEMS	Bias MACC	rmse GEMS	rmse MACC
ABH	-	-	-	-	-	-	-	-	-	-
AMI	41	0.06	0.05	0.07	0.06	25	0.05	0.06	0.07	0.07
ASI	66	-0.06	0.08	0.08	0.09	53	0.01	0.00	0.03	0.03
BET	50	0.02	-0.04	0.08	0.07	29	0.04	-0.01	0.08	0.07
DAK	60	0.01	-0.06	0.22	0.22	83	-0.02	-0.02	0.07	0.06
DAZ	53	0.06	0.00	0.07	0.05	29	0.14	0.12	0.16	0.14
GSF	34	0.11	-0.01	0.12	0.04	48	0.09	-0.01	0.14	0.09
ILO	36	-0.58	-0.56	0.66	0.64	20	-0.09	-0.09	0.18	0.18
KAN	15	-0.28	-0.29	0.40	0.40	47	-0.09	-0.05	0.13	0.14
MEX	-	-	-	-	-	42	-0.16	-0.22	0.23	0.28
MON	26	0.06	0.01	0.11	0.09	64	0.01	-0.02	0.04	0.04
MSU	4	0.11	-0.04	0.12	0.05	35	0.05	-0.01	0.17	0.10
NAU	6	0.01	0.01	0.03	0.05	25	0.02	0.01	0.03	0.03
SAO	22	0.01	-0.05	0.11	0.13	43	-0.10	-0.15	0.16	0.20
SBO	64	0.09	0.05	0.12	0.09	70	0.07	0.05	0.18	0.17
SKU	47	-0.02	-0.03	0.07	0.07	59	-0.02	-0.02	0.05	0.05
SVI	69	0.10	0.08	0.13	0.12	65	0.02	0.07	0.19	0.23
TAH	38	0.01	0.00	0.04	0.03	60	0.00	-0.01	0.03	0.03
TOM	4	0.11	0.01	0.11	0.04	31	0.15	0.10	0.17	0.16
Stn. ID	JUL Nstat	Bias GEMS	Bias MACC	rmse GEMS	rmse MACC	OCT* Nstat	Bias GEMS	Bias MACC	rmse GEMS	rmse MACC
ABH	84	-0.08	-0.10	0.10	0.13	31	-0.27	-0.31	0.43	0.45
AMI	11	-0.01	-0.00	0.05	0.06	23	0.02	0.04	0.05	0.06
ASI	64	0.00	0.00	0.05	0.05	40	0.02	0.01	0.05	0.06
BET	58	-0.01	-0.05	0.04	0.06	39	-0.10	-0.19	0.26	0.33
DAK	89	-0.01	-0.17	0.22	0.28	42	-0.05	-0.07	0.15	0.19
DAZ	45	0.26	0.26	0.28	0.29	45	0.15	0.14	0.15	0.15
GSF	53	0.05	-0.07	0.19	0.17	38	0.08	-0.01	0.12	0.07
ILO	-	-	-	-	-	28	0.03	-0.02	0.10	0.09
KAN	17	0.24	0.26	0.32	0.34	54	-0.17	-0.11	0.27	0.22
MEX	32	-0.16	-0.23	0.22	0.27	31	-0.13	-0.23	0.26	0.32
MON	84	-0.06	-0.07	0.10	0.10	76	-0.15	-0.11	0.22	0.20
MSU*	65	-0.02	-0.07	0.09	0.11	2	0.15	-0.04	0.16	0.04
NAU	15	0.02	-0.01	0.04	0.03	50	0.01	0.02	0.03	0.04
SAO	53	-0.13	-0.17	0.15	0.19	28	-0.10	-0.13	0.21	0.23
SBO*	91	0.11	0.11	0.14	0.14	84	0.11	0.08	0.13	0.10
SKU	73	-0.04	-0.05	0.06	0.07	51	-0.08	-0.07	0.11	0.12
SVI	93	0.14	0.21	0.17	0.25	93	0.05	0.04	0.12	0.12
TAH	31	0.02	0.02	0.05	0.04	56	0.04	0.05	0.06	0.06
TOM	65	-0.03	-0.05	0.12	0.13	11	0.04	0.02	0.06	0.05

*Table 2: The bias and r.m.s. error of the GEMS and MACC τ_{550} relative to the Nstat AERONET measurements in the stations given in Table 1. Data are only given when more than 10 individual AERONET observations are available for the station over a given month. The month respectively refer to January, April, July and October 2003, except where noted * (see Table 1, for Moscow and Sede Boker; see text for the definition of Nstat).*

5 Acknowledgements

Adrian Simmons (ECMWF) and Olivier Boucher (MetOffice, now IPSL-CNRS) are thanked from comments at various stages of the writing of this document.

References

http://dataipsl.ipsl.jussieu.fr/AEROCOM/

http://gems.ecmwf.int/d/products/aer/verif/

http://gems.ecmwf.int/d/products/aer/realtime/

http://www.gmes-atmosphere.eu/d/services/gac/nrt/

Benedetti, A., J.-J. Morcrette, O. Boucher, A. Dethof, R.J. Engelen, M. Fisher, H. Flentjes, N. Huneeus, L. Jones, J.W. Kaiser, S. Kinne, A. Mangold, M. Razinger, A.J. Simmons, M. Suttie, and the GEMS-AER team, 2008: Aerosol analysis and forecast in the ECMWF Integrated Forecast System: Data assimilation. *ECMWF Technical Memorandum*, **571**, 23pp.

Benedetti, A., J.-J. Morcrette, O. Boucher, A. Dethof, R.J. Engelen, M. Fisher, H. Flentjes, N. Huneeus, L. Jones, J.W. Kaiser, S. Kinne, A. Mangold, M. Razinger, A.J. Simmons, M. Suttie, and the GEMS-AER team, 2009: Aerosol analysis and forecast in the ECMWF Integrated Forecast System: Data assimilation. *J. Geophys. Res.*, **114**, D13205, doi:10.1020/2008JD011115.

Boucher, O., M. Pham, and C. Venkataraman, 2002: *Simulation of the atmospheric sulfur cycle in the LMD GCM. Model description, model evaluation, and global and European budgets*. IPSL, Note 23, 26 pp. (available at http://www.ipsl.jussieu.fr/ poles/ Modelisation/ NotesSciences.htm.)

Dee, D., and S. Uppala, 2008: Variational bias correction in ERA-Interim. *ECMWF Technical Memorandum*, **575**, 26 pp.

Dentener, F., S. Kinne, T. Bond, O. Boucher, J. Cofala, S. Generoso, P. Ginoux, S. Gong, J. J. Hoelzemann, A. Ito, L. Marelli, J. E. Penner, J.-P. Putaud, C. Textor, M. Schulz, G. R. van der Werf, and J. Wilson, 2006: Emissions of primary aerosol and precursor gases in the years 2000 and 1750 prescribed data-sets for AeroCom. *Atmos. Chem. Phys.*, **6**, 4321-4344.

Dubovik, O., B. Holben, T.F. Eck, A. Smirnov, Y.J. Kaufman, M.D. King, D. Tanré, and I. Slutsker, 2002: Variability of absorption and optical properties of key aerosol types observed in worldwide locations *J. Atmos. Sci.*, **59**, 590-608.

Holben, B.N., T.F. Eck, I. Slutsker, D. Tanré, J.P. Buis, A. Setzer, E. Vermote, J.A. Reagan, Y.J. Kaufman, T. Nakajima, F. Lavenu, I. Jankowiak, A. Smirnov, 1998: An emerging ground-based aerosol climatology: Aerosol optical depth from AERONET. *J. Geophys. Res.*, **103D**, 12067-12097

Hollingsworth, A., R.J. Engelen, C. Textor, A. Benedetti, O. Boucher, F. Chevallier, A. Dethof, H. Elbern, H. Eskes, J. Flemming, C. Granier, J.W. Kaiser, J.-J. Morcrette, P. Rayner, V.-H. Peuch, L. Rouil, M. Schultz, A. Simmons, and the GEMS Consortium, 2008: The Global Earth-system Monitoring using Satellite and in-situ data (GEMS) project: Towards a monitoring and forecasting system for atmospheric composition. *Bull. Amer. Meteor. Soc.*, **89**, 1147-1164, doi: 10.1175 /2008BAMS2355.1

Huneeus, N., and O. Boucher, 2007: One-dimensional variational retrieval of aerosol extinction coef-

ficient from synthetic LIDAR and radiometric measurements. *J. Geophys. Res.*, **112**, D14303, doi: 10.1029 /2006/JD007625.

Huneeus, N., M. Schulz, Y. Balkanski, J. Griesfeller, S. Kinne, J. Prospero, S. Bauer, O. Boucher, M. Chin, F. Dentener, T. Diehl, R. Easter, D. Fillmore, S. Ghan, P. Ginoux, A. Grini, L. Horowitz, D. Koch, M.C. Krol, W. Landing, X. Liu, N. Mahowald, R. Miller, J.-J. Morcrette, G. Myhre, J. Penner, J. Perlwitz, P. Stier, T. Takemura, and C. Zender, 2011: Global dust model intercomparison in AEROCOM phase I. *Atmos. Chem. Phys.*, **11**, 7781-7816, doi:10.5194/acp-11-7781-2011.

Kaiser, J.W., M. Suttie, J. Flemming, J.-J. Morcrette, O. Boucher, and M.G. Schultz, 2009: Global real-time fire emission estimates based on space-borne fire radiative power observations. *AIP Conf. Proc.*, **1100**, 645-648.

Kaiser, J. W., A. Heil, M.O. Andreae, A. Benedetti, N. Chubarova, L. Jones, J.-J. Morcrette, M. Razinger, M.G. Schultz, M. Suttie, and G.R. van der Werf, 2011: Biomass burning emissions estimated with a global fire assimilation system based on observed fire radiative power. *Biogeosciences Discuss.*, **8(4)**, 7339-7398.

Mangold, A., H. De Backer, B. De Paepe, S. Dewitte, I. Chiapello, Y. Derimian, M. Kacenelenbogen, J.-F. Lon, N. Huneeus, M. Schulz, D. Ceburnis, C. O'Dowd, H. Flentje, S. Kinne, A. Benedetti, J.-J. Morcrette, and O. Boucher, 2011: Aerosol analysis and forecast in the European Centre for Medium-Range Weather Forecasts Integrated Forecast System: 3. Evaluation by means of case studies, *J. Geophys. Res.*, **116**, D03302, doi: 10.1029 /2010JD014864.

Morcrette, J.-J., O. Boucher, L. Jones, D. Salmond, P. Bechtold, A. Beljaars, A. Benedetti, A. Bonet, J.W. Kaiser, M. Razinger, M. Schulz, S. Serrar, A.J. Simmons, M. Sofiev, M. Suttie, A.M. Tompkins, A. Untch, 2009: Aerosol analysis and forecast in the ECMWF Integrated Forecast System: Forward modelling. *J. Geophys. Res.*, **114**, doi: 10.1029 /2008JD011235.

Reddy M. S., O. Boucher, N. Bellouin, M. Schulz, Y. Balkanski, J.-L. Dufresne, M. Pham, 2005: Estimates of global multicomponent aerosol optical depth and direct radiative perturbation in the Laboratoire de Meteorologie Dynamique general circulation model, *J. Geophys. Res.*, **110D**, S16, doi: 10.1029 /2004JD004757.

Rodwell, M.J., and T. Jung, 2008: Understanding the local and global impacts of model physics changes: An aerosol example. *Quart. J. Roy. Meteor. Soc.*, **134**, 1479-1497, doi: 10.1002/qj.298

Shi, Y., J. Zhang, J. S. Reid, B. Holben, E. J. Hyer, and C. Curtis, 2011: An analysis of the collection 5 MODIS over-ocean aerosol optical depth product for its implication in aerosol assimilation. *Atmos. Chem. Phys.*, **11**, 557-565.

Simmons, A.J., 2010: Monitoring Atmospheric Composition and Climate, *ECMWF Newsletter*, **123**, 10-13.

Tanré, D., J.-F. Geleyn, and J.M. Slingo, 1984: First results of the introduction of an advanced aerosol-radiation interaction in the ECMWF low resolution global model, in *Aerosols and their Climatic Effects*, H.E. Gerber and A. Deepak, eds., A. Deepak Publishing, Hampton, Va, USA, 133-177.

Tegen, I, P. Hoorig, M. Chin, I. Fung, D. Jacob, and J. Penner, 1997: Contribution of different aerosol species to the global aerosol extinction optical thickness: Estimates from model results. *J. Geophys. Res.*, **102**, 23,895-23,915.

Tompkins, A.M., 2005: *A revised cloud scheme to reduce the sensitivity to vertical resolution*. ECMWF Research Dept Technical Memorandum, 20 pp.

Tompkins, A.M., C. Cardinali, J.-J. Morcrette, and M. Rodwell, 2005: Influence of aerosol climatology on forecasts of the African Easterly Jet. *Geophys. Res. Letters*, **32**, L10801, doi: 10.1029 /2004GL022189.

van der Werf, G.R., J.T. Randerson, L. Giglio, G.J. Collatz, M. Mu, P.S. Kasibhatla, D.C. Morton, R.S. DeFries, Y. Jin, and T.T. van Leeuwen, 2010: Global fire emissions and the contribution of deforestation, savanna, forest, agricultural, and peat fires (1997-2009). *Atmos. Phys. Chem.*, **10**, 11707-11735, doi: 10.5194/acp-10-11707-2010.